

CHAPTER 2

Chapter 2

Issues arising from experimental and human errors

SUMMARY

This chapter starts with the account of data and software used in the study. It also mentions about the study areas for which the spectral observations were made. Then, it consists of a detailed discussion on the inherent quality issues with special reference to the following- Understanding the influence of smile effect, band-to-band registration and noise in data over vegetation assessment. It includes how the judgement of radiance values for vegetation lead to addressing and improvement in response of the airborne hyperspectral sensor. It also includes the understanding based upon the studies pertaining to the effect of exposure time on vegetation's radiance values, saturation radiance, insufficient sampling, presence of stacks of leaves, phenological stage, species and variety of vegetation through studying the vegetation spectra.

BACKGROUND

The presence of large number of bands, the inherent issues with hyperspectral remote sensors and the lack of understanding of some of the principles underlying hyperspectral data interpretation, lead to the mis-interpretation of the data and hence misleading results. Christophe et al (2005) conducted a comprehensive study on comparison and evaluation of quality criteria for hyperspectral imagery. These criteria were mainly meant for sensor's performance in the laboratory and hold little relevance with the image. Since,

image is usually the only means for assessing hyperspectral data quality for the application scientist, systematic understanding of the quality issues need to be addressed. Christophe et al. (2005) indicated that for hyperspectral images, quality criteria have to be relevant to the corresponding applications.

There are three critical elements of an Imaging Spectrometer:

- Uniformity
- Radiometric Precision or Signal-to-Noise-Ratio.
- Calibration

Uniformity is required for spectroscopy in the image domain. The second critical element is radiometric precision or SNR. High precision is critical as is required to answer questions of relevance in imaging spectroscopy. Low precision undermines detection, identification, quantification and monitoring. The third critical element is spectral, radiometric and spatial calibration which is important in imaging spectroscopy. These are some factors, apart from the factors like image corruption due to atmospheric effects or due to experiment design etc. It may be seen that numerous factors corrupt the hyperspectral image at various levels. How and to what extent these factors play their role in various capacities, is discussed in the following text.

2.1 DATA AND SOFTWARE USED

For analyzing various aspects of hyperspectral data for vegetation assessment, the data used was from all of the three types of platforms, viz. airborne (AIMS, AHySI), spaceborne (Hyperion, HICO) and hand-held (ASD Spectroradiometer). Moreover, the

observations using these instruments was performed over a number of sites. This ensured inclusion of dynamicity within the vegetation category. *The same datasets, as well as the study areas are used for the analysis in the forthcoming chapters as well.*

2.1.1 Hyperion

Hyperion is a space borne push-broom sensor, onboard NASA’s EO-1 satellite (<https://eo1.gsfc.nasa.gov>). It has 242 bands in 400nm-2500nm range of electromagnetic spectrum, at an average resolution of 10nm. The data selected was of level 1Gst. The Gst data level is radiometrically corrected and orthorectified. Table 2.1 lists some of the important characteristics of the sensor.

Table 2.1: Hyperion data specifications

Number of bands	242 (196 calibrated and unique bands)
Spectral range (nm)	400-2500
Spatial resolution	30m
Swath	7.5 km
GSD	30m
Quantization	12 bit
Orbit height	705 km

2.1.2 Hyperspectral Imager for Coastal Oceans

Hyperspectral Imager for Coastal Ocean (HICO) sits over the International Space Station (ISS) and is largely meant for scientific research related to the coastal studies, though it

may be very well used for terrestrial applications. Table 2.2 briefly describes the HICO specifications (www.hico.coas.orgonstate.edu).

Table 2.2: HICO specifications

Parameter	Specification
Spectral Range	350-1080nm
Spectral Channel width (Normal mode)	5.7nm
SNR	>200:1 for 5% albedo target
Nadir cross track GSD	94m@400km
Nadir along-track GSD	99m
Scene size	42km x 192 km
Saturation	Does not saturate when viewing 95% albedo cloud

2.1.3 Airborne Imaging Spectrometer

India's Airborne IMaging Spectrometer (AIMS) is a hyperspectral imager with 143 bands in the spectral range of 456 to 882nm within the electromagnetic spectrum (Anon, 1993). It has a nominal spatial resolution of 4.8m while spectral resolution of 3nm. Being airborne, it is flown at different heights, as per the requirement. In this case, flight altitude was 6.5 km. Table 2.3 briefs the specifications of AIMS.

Table 2.3: AIMS specifications

Average Flight Altitude	6.5km
Swath	1.84km
Nominal Resolution	4.8m
Spectral range	459-885nm
Number of bands	143
Spectral Sampling Interval	3nm

2.1.4 HyperSpectral Imager- Spaceborne and Airborne

Hyper Spectral Imager (HySI) is a hyperspectral imaging remote sensor flown on-board Chandrayaan-1, India's first mission to moon as well as on IMS-1 (Indian Mini Satellite) for Earth observations. The data used here for analysis is acquired by flowing HySI on-board IMS-1. HySI has 64 contiguous bands in the VNIR region, in the spectral range of 0.4-0.95 μm and exhibits spectral resolution of better than 15 nm and spatial resolution of 505.6 m with swath coverage of 129.5 km (Kumar, 2008). The same instrument was flown on airborne platform also. In that case, it is called Airborne HySI (AHySI). The airborne adaptation has 512 contiguous bands. The spatial resolution is around 4.8m. Here, different bands of the instrument do not acquire the image of a given feature simultaneously. Successive bands look at the same feature with a time interval of around 51.8ms. Tables 2.4 and 2.5 respectively list some of the specifications of HySI and AHySI.

Table 2.4: HySI specifications

Average Flight Altitude	~720km
Swath	129.5 km
Nominal Resolution	505.6m
Spectral range	0.4-0.95 μm
Number of bands	64
Spectral Sampling Interval	15nm

Table 2.5: AHySI specifications

Average Flight Altitude	6.9 km
Nominal Resolution	4.8 m
Spectral range	0.4-0.95 μm
Number of bands	480 (calibrated)

2.1.5 Hand-held Spectroradiometer

The hand-held Spectroradiometer used had 2151 channel within the spectral range of 350–2500 nm. The instrument acquired hyperspectral data at a spectral resolution of 3 nm at 25° field of view. However, by re-sampling the instrument provided data at 1 nm interval. Table 2.6 shows the main characteristics of the Spectroradiometer (ASD technical guide).

Table 2.6: Characteristics of hand-held Spectroradiometer

Spectral Range	350-2500 nm
Spectral Resolution	3 nm @ 700 nm; 10 nm @ 1400/2100 nm
Sampling Interval	1.4 nm @ 350-1050 nm; 2 nm @ 1000-2500 nm
FOV	25° field of view
Scan Time	100 milliseconds

2.1.6 Image processing software

Environment for Visualizing Images (ENVI) is an image processing software, used to process and analyze geospatial imagery. It has Interactive Data Language (IDL) in its backdrop. Version 4.4 of ENVI-IDL was used for processing images in this work.

2.1.7 Data simulation software

The simulation studies corresponding to Phytoplankton was carried out using Coupled Ocean and Atmosphere Radiative Transfer (COART) model (Jin & Stamnes, 1994; Jin et al., 2006). It was a freeware online model. This tool calculates radiance and reflectance at many levels in the atmosphere and ocean and at various view and zenith angles. Varying levels of wind speed and chlorophyll could be set. In this model, when Ocean depth is set to 0, it reduces to the conventional atmospheric radiative transfer model.

2.1.8 Statistical software

For carrying out statistical computations and analysis, especially Step wise discriminant analysis and ANOVA, Statistical Package for the Social Sciences (SPSS) version 16 (SPSS, 2007) was used. It is an interactive package for statistical analysis and is quiet user friendly.

For identifying peaks in the hyperspectral data, peak fitting module of Origin Lab software was used. It is a proprietary computer program for interactive scientific graphics and data analysis.

2.1.9 Spectra analysis software

The spectra were evaluated through an in-house developed software ‘Spectral Analysis’ (Sanghvi et al., 2010). It is a free software tool designed to analyze the spectral

reflectance profiles. It can perform spectral averaging, remove continuum, generate derivative spectra, perform red edge analysis, smoothen curves, compute vegetation indices and generate folded spectra corresponding to other sensors according to their RSR. Some part of the spectral analysis was done by MS Excel.

2.2 STUDY AREAS

In order to account for the diversity in vegetation, five categories were studied. These include Mangroves, which essentially grow in the coastal saline regions; Tropical forests, which form the major composition of India's forest types; Agricultural crops, which should have the maximum stake in hyperspectral remote sensing; Crop residue, which confuses with the other farm components when viewed from space and the ocean's primary producers-Phytoplanktons. For each category, the study areas were different. The details are listed below.

2.2.1 Bhitarkanika reserve forest

This Reserve Forest lies in Kendrapara district in Orissa, India and forms the core area of Bhitarkanika mangrove forest. Figure 2.1 shows the study area. *Heritiera fomes* is the dominant species of this area (Upadhyay and Misra, 2008). Hyperion data was used for analyzing the mangrove forest. Additionally, hand-held Spectroradiometer observations were made for some of the mangrove species within the nursery plantation. This includes observations for *Avicennia officinalis*, *Bruguiera gymnorrhiza*, *Lumnitzera racemose*,

Bruguiera cylindrical, *Aegiceras corniculatum*, *Sonneratia apetala*, *Amoora cucullata*, *Cerbera manghus* and *Rhizophora stylosa*.

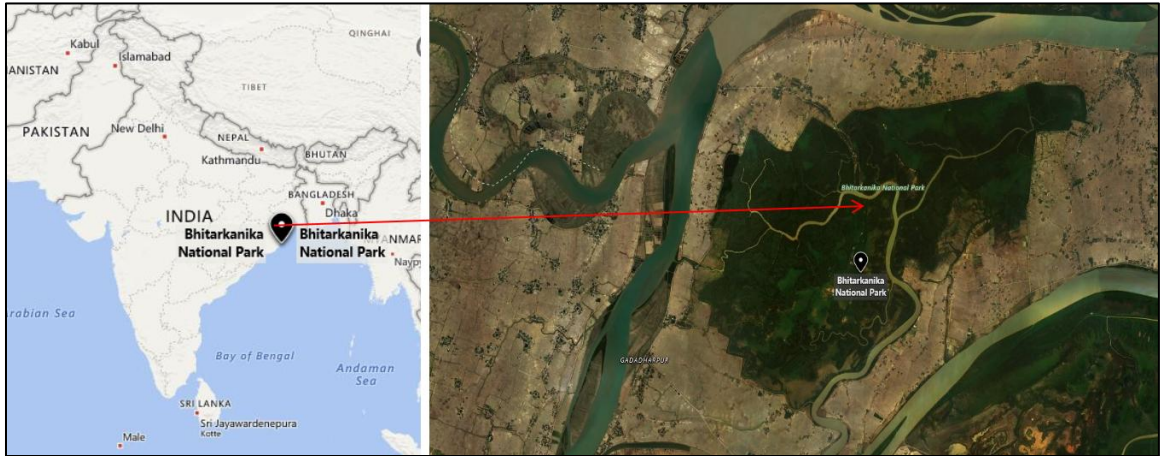


Figure 2.1: Bhitarkanika reserve forest. Here observations were made using handheld Spectroradiometer. Hyperion data was also used.

2.2.2 Jamnagar mangrove forest

This study area comprises of mangrove vegetation along with mangrove associates in the creek, salt pans, and mudflat near the Rozi bet in Jamnagar, Gujarat, which is a part of the Gulf of Kutch Marine National park. The study area is dominated by *Avicennia marina*. *Prosopis juliflora* is found towards inland region. Mud flats saturate highly with sea water during high tides. Airborne hyperspectral data was used for this study site. Figure 2.2 shows the study area and its surroundings.

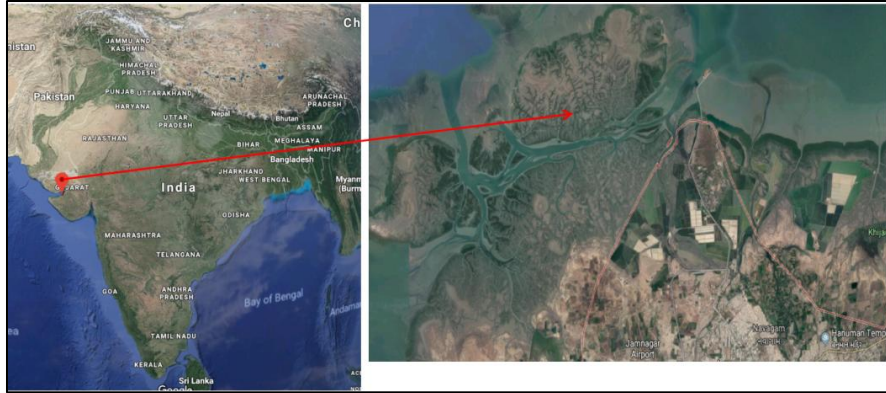


Figure 2.2: Jamnagar mangrove forests and surroundings. Here observations were made using hand-held Spectroradiometer. AIMS and AHySI data were also used.

2.2.3 Forest Research Institute, Dehradun, Uttarakhand

The experimental plots of Forest Research Institute, Dehradun, Uttarakhand, India are typical representative of some of the country’s major forest species i.e. Chir pine (*Pinus roxburghii*), Tropical Pine (*Pinus caribea*), Teak (*Tectona grandis*), Sal (*Shorea robusta*), Saza (*Terminalia tomentosa*) and Eucalyptus (*Eucalyptus hybrid*). Figure 2.3 shows the study area. Hyperion data was analyzed for this study site.

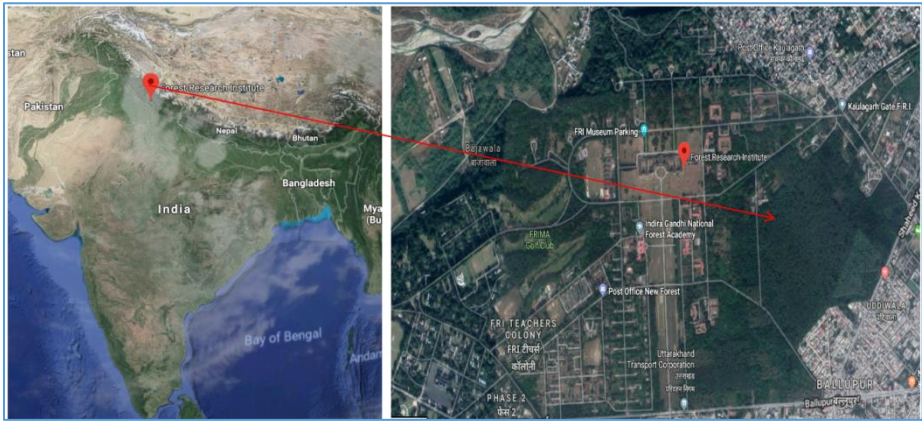


Figure 2.3: FRI, Dehradun. Hyperion data was used for this area.

2.2.4 Laboratory spectra

Spectral Measurements of Juvenile, mature and young leaves of nine tropical species, collected using Hand-held Spectroradiometer observations from the campus of Maharaja Sayajirao University of Baroda, Gujarat, India were used in this study. The tropical forest species included *Tectona grandis* (Teak), *Mangifera indica* (Mango), *Ficus glomerata* (Ficus), *Syzigium commune* (Jamun), *Dendrocalamus strictus* (Bamboo), *Madhuca indica* (Madhuca), *Butea monosperma* (Butea), *Azadirachta indica* (Neem) and *Mitragyna parvifolia* (Mitragyna). Leaves, healthy and homogeneous in color without any visible symptoms of damage, were used in the experiments.

2.2.5 Research farm at Anand Agricultural University

Research farm of Anand Agricultural University comprises of more than twenty types of agricultural crops. Apart from the crop variety, the agricultural plot had more than six kinds of paddy. All varieties of paddy were in tillering stage (8 tillers on an average), had an average height of 60cm and ground cover of almost 50%. Other crops included *Sorghum bicolor* (Sorghum, ear bearing stage), *Vigna radiata* (green gram, fruiting stage), *Macrotyloma uniflorum* (horse gram, flowering stage), *Cajanus cajan* (pigeon pea, young), *Vigna unguiculata* (cow pea, pod formation stage), *Sesbania bispinosa* (dhaincha, young), *Sachharum officinarum* (sugarcane, mature), *Gosypium* (Cotton, mature), *Beucarnia recurvate* (elephant foot, mature), *Curcuma longa* (turmeric, mature), *Arachis hypogaea* (groundnut, mature), *Glycine max* (soybean, pod formation stage), *Sesamum indicum* (sesamum, pod formation stage), *Helianthus* (sunflower, flowering

stage) and *Ricinus communis* (castor, mature). The crop cover was almost 90%, in fact, better than that in some cases. For all of these crops, the spectra were collected using hand-held Spectroradiometer. Figure 2.4 gives a picture of the study site.



Figure 2.4: Field pictures of groundnut and sesamum grown in AAU, Anand.

Spectroradiometer observations were made for crops at AAU.

2.2.6 Jalandhar, Punjab, India

The study was carried out at the experimental farms of Central Potato Research Station (CPRS) as well as at the Farmers' fields located at Jalandhar, Punjab (figure 2.5a). Also shown are the field photographs of various stages of wheat crop grown there (figure 2.5b). During the time of observation wheat was the major crop at different phenological stages. The spectra for different stages was taken using hand-held Spectroradiometer.

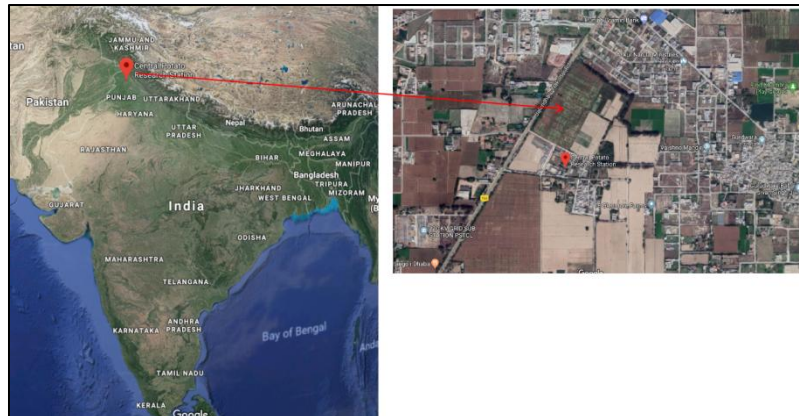


Figure 2.5a: CPRS, Jalandhar, Punjab. Spectroradiometer observations were made for crops here

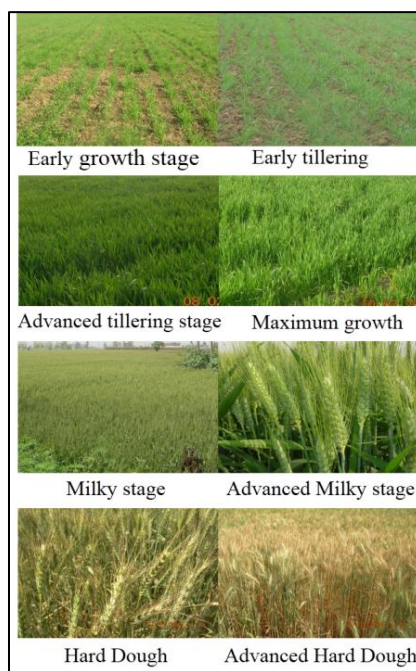


Figure 2.5b: Field photographs of various stages of wheat crop

2.2.7 Agricultural fields of Moga and Naraingarh areas of Punjab

Study was also conducted over agricultural fields of Moga and Naraingarh areas of Punjab state of India during the period of Wheat harvest. The crop is harvested either

manually or by a combine followed by a reaper. Hence, at any particular time during harvesting period, one can find fields with standing matured crops; combine, reaper and hand harvested fields and fallow lands. The soil type of Punjab is mostly sandy loam. So, hand-held Spectroradiometer observations were obtained for wheat residue, harvested through various techniques like combine harvesting, hand-harvesting and through combine and reaper. Figure 2.6 shows the location of the study site.

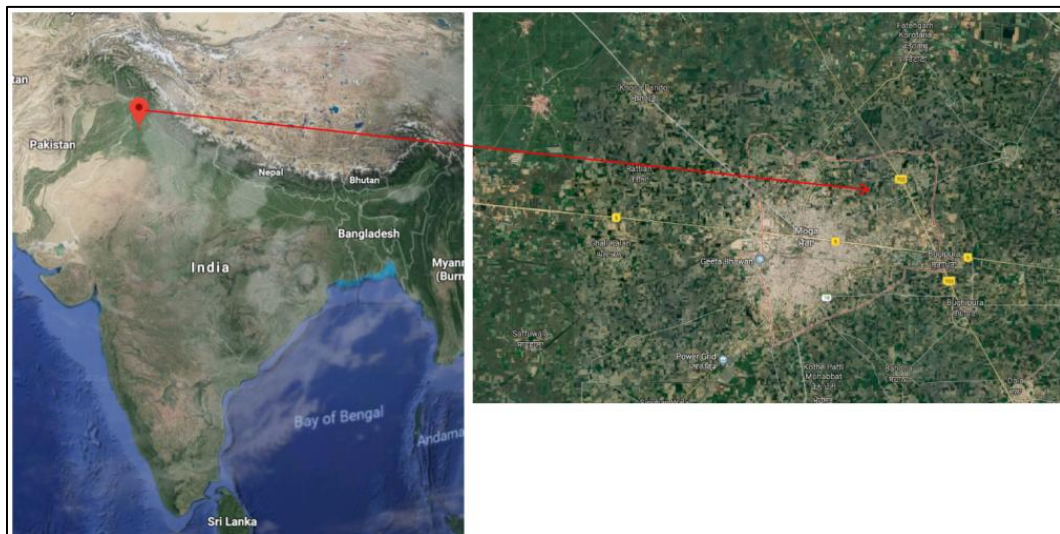


Figure 2.6: Location of farms at Moga, Punjab. Spectroradiometer observations were made for crops here.

2.2.8 Anonymous sites

For sensors AIMS, HySI, HICO and AHySI, anonymous sites were also taken. Some of them were among the test runs of airborne flights. They were mainly from the states of Gujarat and Karnataka.

2.3 QUALITY CHECK FOR INHERENT ISSUES WITH HYPERSENSPECTRAL DATA FOR VEGETATION ASSESSMENT

The typical reflectance spectra of vegetation have many troughs and peaks showing the presence of pigments like chlorophyll and also absorption by gases and water. An example is shown in figure 2.7. The characteristic chlorophyll dips are shown at ~430/450 nm, 660/680nm and peak at 550nm. It also shows high reflectance in NIR region and especially the sharp inflexion point of red edge (~670nm), although in different cases the position of inflexion point ranges between 670 to 720nm. Typical plant reflectance is shown along VNIR region and then strong water absorption at ~970nm, ~1400nm, ~1940nm. The presence of such sharp absorptions and peaks reflecting corresponding major characteristics clearly indicate that any shift from any of these wavelengths will create havoc in data interpretation and the final outcome.

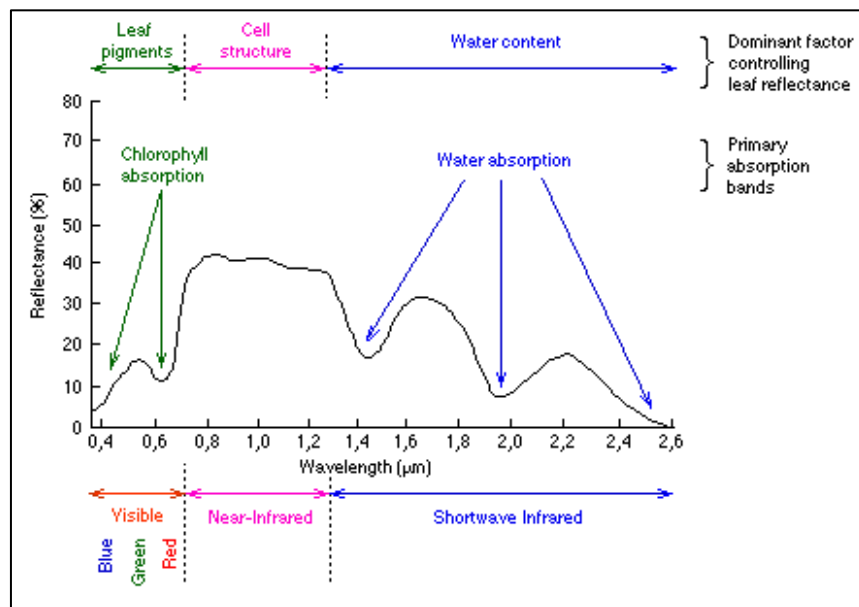


Figure 2.7: Figure showing various absorption regions in vegetation spectrum

(Source: www.senteksystems.com)

2.3.1 Understanding the influence of smile effect

Many times, visual inspection of hyperspectral images reveal gradient in brightness along different parts of the image, as shown in figure 2.8. Sometimes, this gradient is not easily perceived through naked eye. Nonetheless, in both the cases, a shift in bands from their ostensible positions may exist. This effect is smile or frown effect. The shifted bands corrupt the information extracted from them. This is because different molecules/atoms of the target under study have absorption in unique wavelengths and forms a characteristic feature of that particular target. With change in positions of the characteristic wavelengths, the diagnosis of the target falls under suspicion. To make the situation worse, smile effect changes with time (Neville et al., 2008). Hence, it needs to be detected and reported before any meaningful interpretation is done.

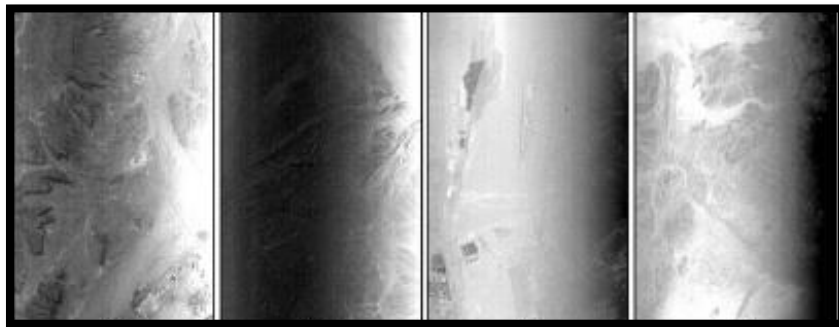


Figure 2.8: Smile effect shown in different bands of hyperspectral images, extracted from AIMS and Hyperion

2.3.1.1 Method

The atmospheric gas absorption features are very sharp and errors in wavelength calibrations can produce significant errors in the retrieved land or ocean surface

reflectance around these features (Gao, 2004). The narrow oxygen absorption feature centered on 762 nm can be effectively used for assessing spectral calibration. Any shift in absorption band from 762nm signify the presence of smile. To use this characteristic wavelength for smile detection, a large number of Regions of Interest (ROIs) having 9 pixels each (3*3) were taken at constant interval along the horizontal transect of the image. For each ROI, mean DN/radiance values were computed. The mean value accounts for the minor variability in the immediate neighboring pixels. For each ROI, the spectral plot was generated. Using peak fitting module of Origin Lab software, the peaks and dips were recorded for each spectrum. Following this, deviation from 762nm was plotted for each ROI.

Once, smile effect is detected, a few questions arise-1) Does smile effect influence the whole image in equal amount? 2) Can bias correction be done or an image based model be fitted to account for smile effect? 3) Does smile affect all kinds of targets equally? and 4) What implication does smile effect have on vegetation assessment?

To cater to questions 1 and 2, smile detection is done at three portions of the image-upper, middle and bottom. For question 3, ratio spectra were generated for three kinds of target-soil, mangrove and mudflat. Here, the original spectrum is shifted by 1nm and then the ratio is computed between the original and shifted spectrum. Lastly, for studying the impact of smile effect on vegetation, a case study corresponding to different mangrove species was done. Here, red edge inflection point was recorded for each species. Red edge is the region of sudden change in reflectance of healthy green vegetation from visible to NIR region. It is found through computation of maxima in first derivative spectra.

To study smile effect, analysis was done for the two datasets, namely AIMS and AHySI. For case study, Spectroradiometer observations were taken.

2.3.1.2 Results and Discussions

The airborne or spaceborne data goes through a series of processing steps before it becomes available to the user domain. At each step, the data quality is assessed and reported for further improvement (if any). In this light, AIMS as well as AHySI data were taken at various processing levels and were thoroughly analyzed for the presence of smile effect. Here, the Oxygen absorption wavelength method (as discussed above) was adopted. Figure 2.9 shows AHySI and AIMS datasets along with the deviation from 762nm for across track ROIs.

Visually, the brightness gradient is not apparent in both the images. When deviation from 762nm is plotted, AHySI data reveals shift in wavelengths from center towards right. The deviation is as high as 4.5nm, although at a few points the deviation falls to 0. The presence of smile is rather random in this case. For AIMS dataset, the deviation of as high as 3.3nm exists along the two sides of the image. At the center, deviation is close to 0 i.e. bands are not shifted. This kind of smile effect is somewhat similar to that of CASI, as reported by Jacobsen et al. (2000).

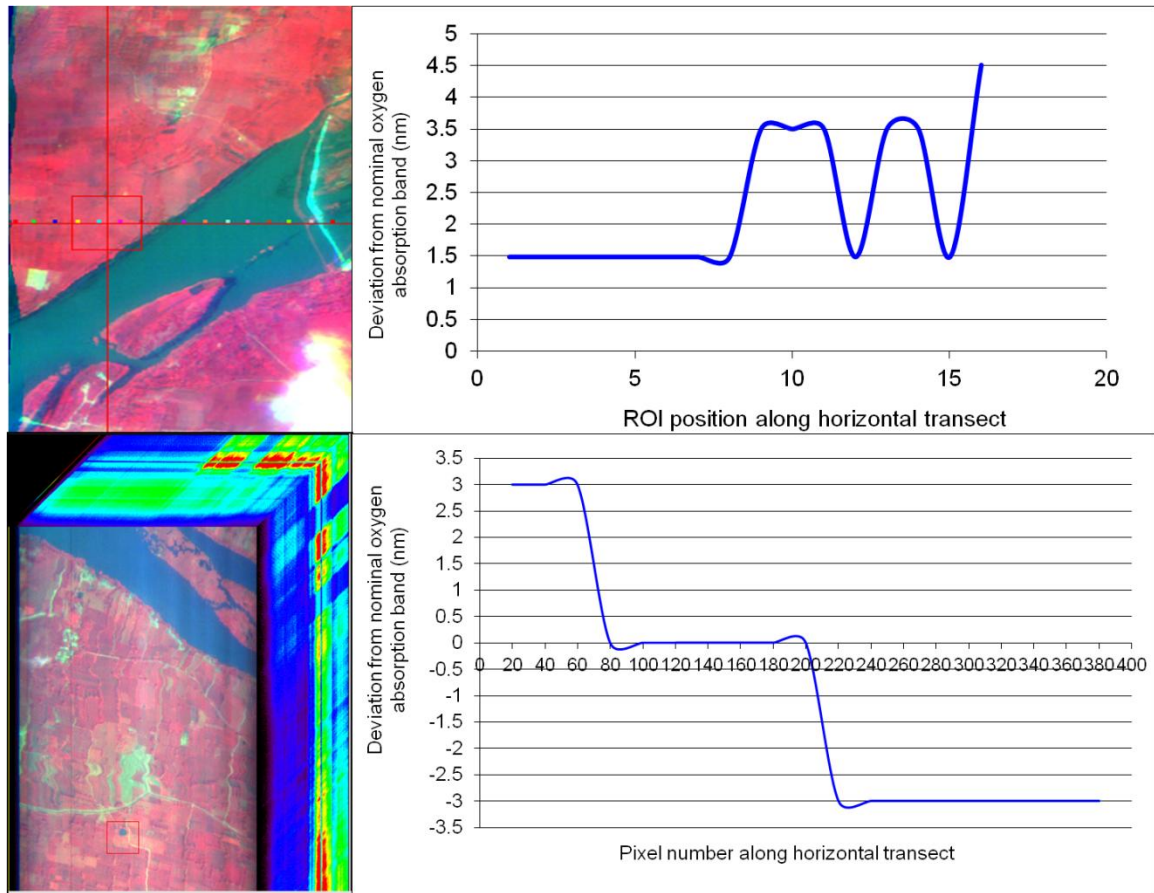


Figure 2.9: AHySI data, Mysore (top) and AIMS data, Mysore (bottom) along with the deviation from oxygen absorption channel track plotted for pixels across track

It may be concluded here that *Smile effect can be present in variable proportions across the image. Since, deviation can be positive as well as negative, so, no simple bias correction can be done. Also, since deviation does not follow any order. This poses limitation on fitting of empirical model to rectify these wavelength shifts.*

Now, the point of concern is whether smile effect change with data to data? To answer this query, another AIMS dataset was taken for which the same exercise was performed i.e. finding the spectral profile for across track ROIs. The deviation from ostensible

wavelengths for these spectral profiles for the pixels across track are plotted, shown in figure 2.10. Completely different from what was observed in figure 2.9, this set of data showed deviation throughout the image in varying proportions (Figure 2.10-above). *This made one thing clear that smile effect should be checked every time before use as no two datasets have same level of smile.* When this input was provided, AIMS data was corrected within the processing chain. The resulting image was again checked for smile. This time the image was corrected, smile per se (Figure 2.10-below). *Thus, smile effect can be corrected at processing level.*

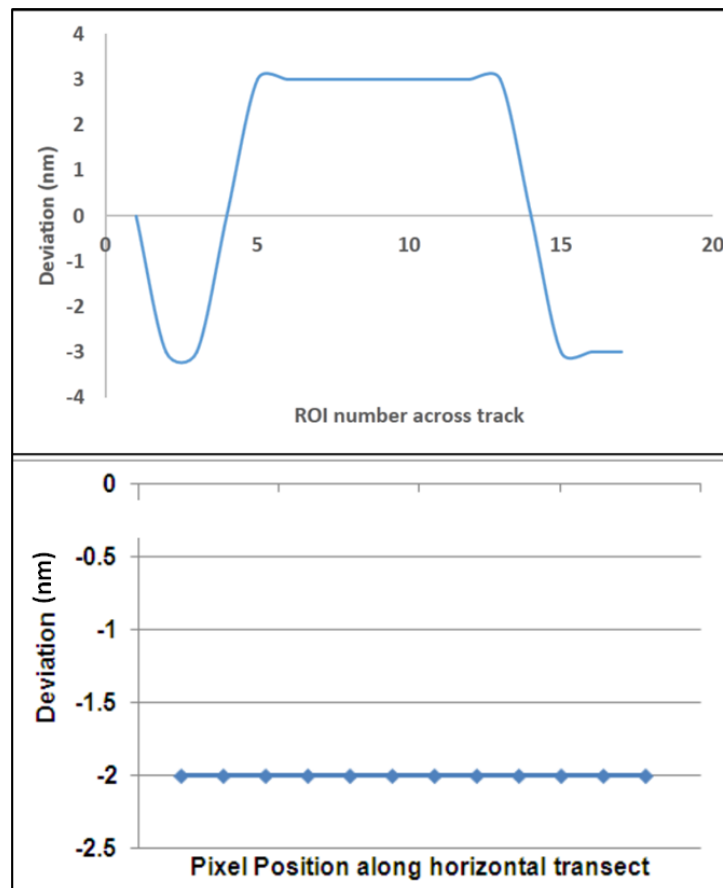


Figure 2.10: Deviation from oxygen absorption wavelength plotted for AIMS data before smile correction (above) and after smile correction (below)

One thing is clear from the above discussion that smile effect exists across the image. To understand its presence along the vertical dimension of the image, AHySI image was studied along the three parts -Upper, Middle and Lower. The spectral profiles of across track ROIs are plotted along with the deviation from the typical Oxygen absorption wavelength (figure 2.11).

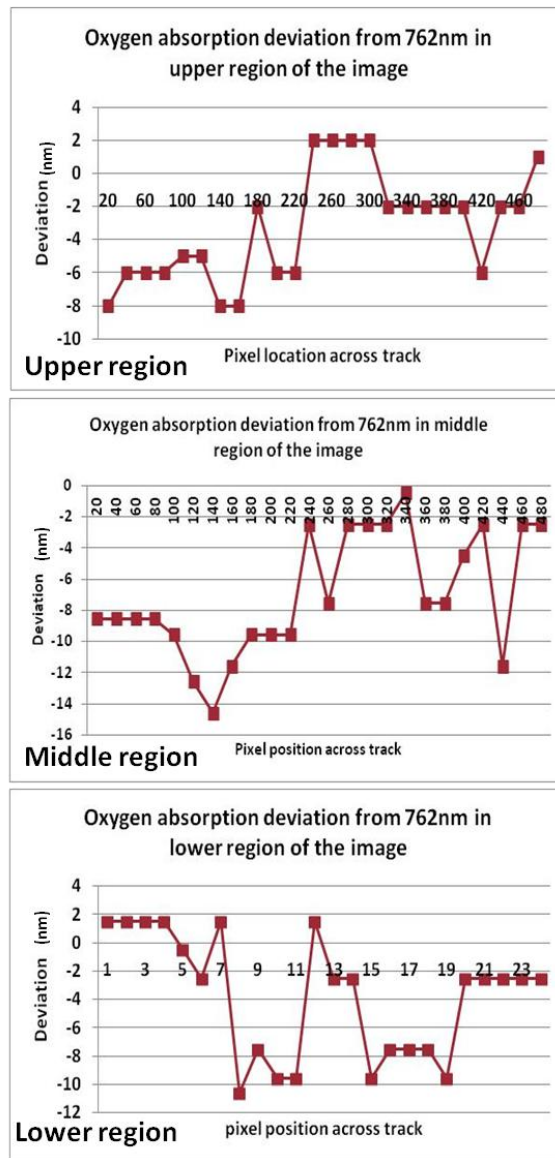


Figure 2.11: Deviation from oxygen absorption wavelength plotted for showing presence of smile in AHySI data along the three sections of the image

No doubt, in three parts of the image smile appears to be varying as is visible through figure 2.11. But, the level of deviation is significantly high which goes to as much as 16nm. This indicates a call for reanalysis of Look Up Tables and rework in processing chain, which was later done. Yet, the point for which this investigation was done was not clear. So, corrected AIMS data as well as Hyperion data were also analyzed. The resulting plots showing deviation are shown in figure 2.12.

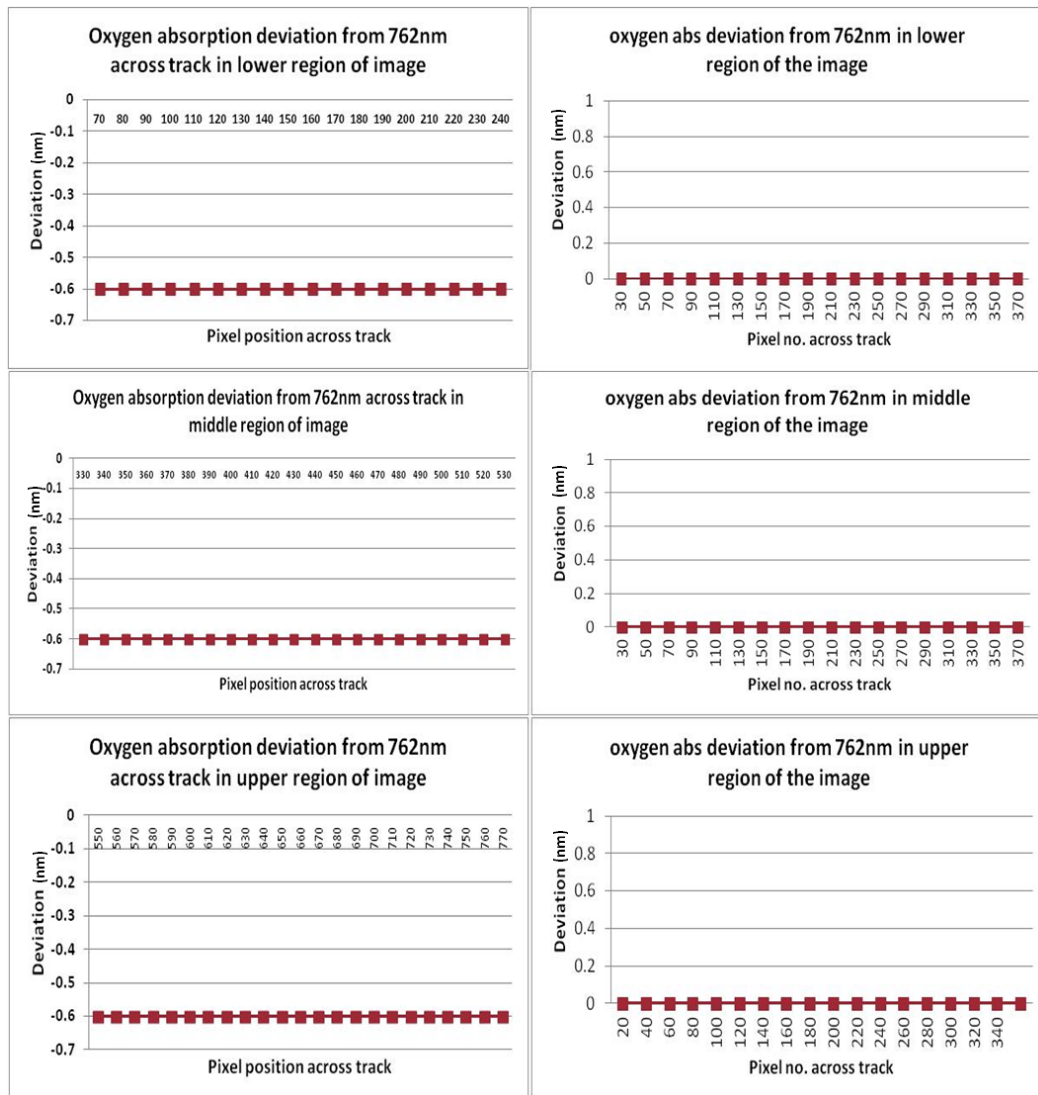


Figure 2.12: Smile detection in Hyperion (left) and AIMS (right) for three parts of the image

Figure 2.12 summarizes that smile changes across track but along the image the variation is constant.

Now, once it is clear that how and to what level smile affects the data, it is relevant to know its consequence on vegetation. So, spectra of two ROIs representing the same tree species were taken from AIMS data (AIMS data before smile correction). The plot is shown in figure 2.13. Here, due to smile, the oxygen absorption channel is shifted in both the cases and occurs at 758nm and 764nm respectively. This has resulted in the shift in ‘red-edge’ region in both the cases, although the species type, vegetation condition and phenological age are the same for both the cases. The consequence is- *smile can lead to wrong identification of the vegetation type and its condition.*

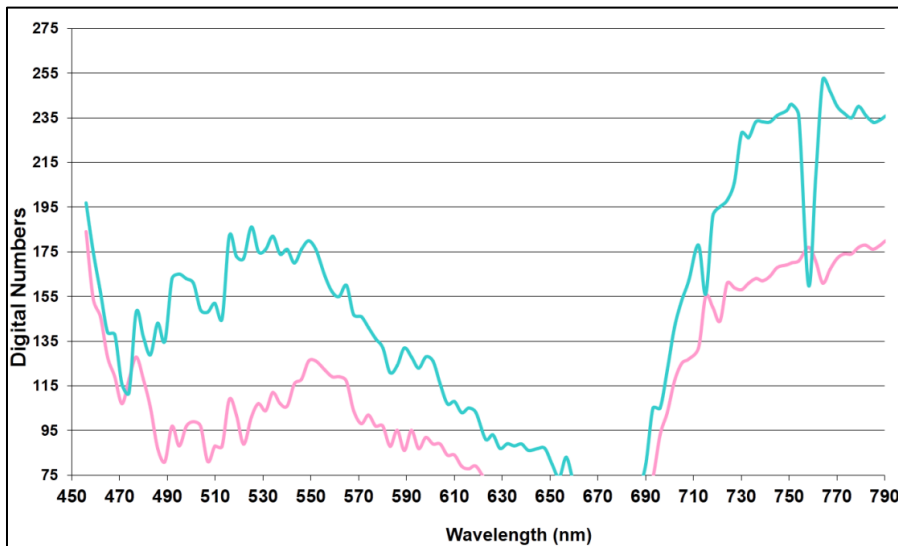


Figure 2.13: Spectral plots of different ROIs of same tree species of AIMS data

Furthermore, to illustrate upon the wrong assumptions made due to the presence of smile, spectral plots for a few mangrove species were studied. The spectra (shown in figure

2.14) look similar in pattern within the visible range of the spectrum but as soon as they hit the red edge region, the story changes. Each spectrum, on account of its species, stage and condition, show variation in the inflection point of the red edge which essentially remains in the 680-730nm range. For all of these species, the inflexion point is shown in table 2.7.

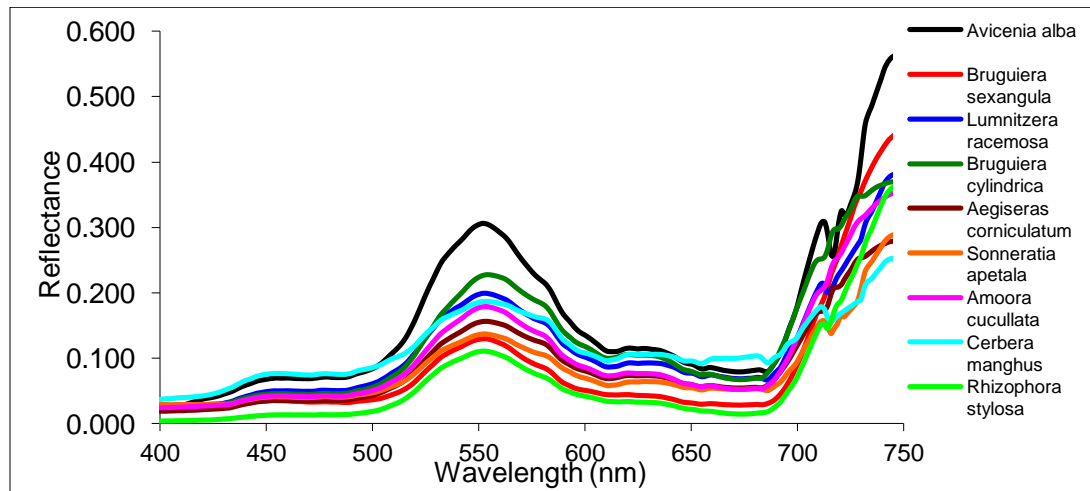


Figure 2.14: Spectral plots for mangrove species taken using Spectroradiometer at Bhitarkanika RF

Table 2.7: Red edge inflexion point of mangrove species

Mangrove species	Inflection point (nm)
<i>Avicennia officinalis</i>	732
<i>Bruguiera gymnorrhiza</i>	718
<i>Lumnitzera racemosa</i>	731
<i>Bruguiera cylindrica</i>	656
<i>Aegiceras corniculatum</i>	707
<i>Sonneratia apetala</i>	733
<i>Amoora cucullata</i>	703
<i>Cerbera manghus</i>	746
<i>Rhizophora stylosa</i>	727

From the table above, it can be seen that these inflexion points are very specific. Also, they lie near to each other. The smile effect which not only changes the ostensible band position in varying numbers but also changes in a random manner across the image, confuses the identification and discrimination of the vegetation species. For example, a shift of 4nm can lead to confusion between *Rhizophora stylosa* and *Lumnitzera racemosa* or between *Amoora cucullata* and *Aegiceras corniculatum*. This is in line with the study by Dadon et al. (2009) who showed problems in classification results owing to smile affected Hyperion data use.

At last, one more question arises that whether smile is a problem with all kinds of land covers or does it affect vegetation more? To answer this question, hand-held Spectroradiometer observations were made for three land cover classes-soil, mangroves and mudflats. Then, all the kinds of spectra were shifted by 1nm and the ratio spectra were plotted (shown in figure 2.15). While soil and mudflat hardly showed any variation within the spectral range under study (probably because the constituting minerals in them have absorptions at higher wavelengths), vegetation spectra show the presence of many peaks and dips. This makes it clear that while for soil and mudflat, it really does not matter much but *for vegetation, the shift in bands is of higher significance in the spectral range under study.*

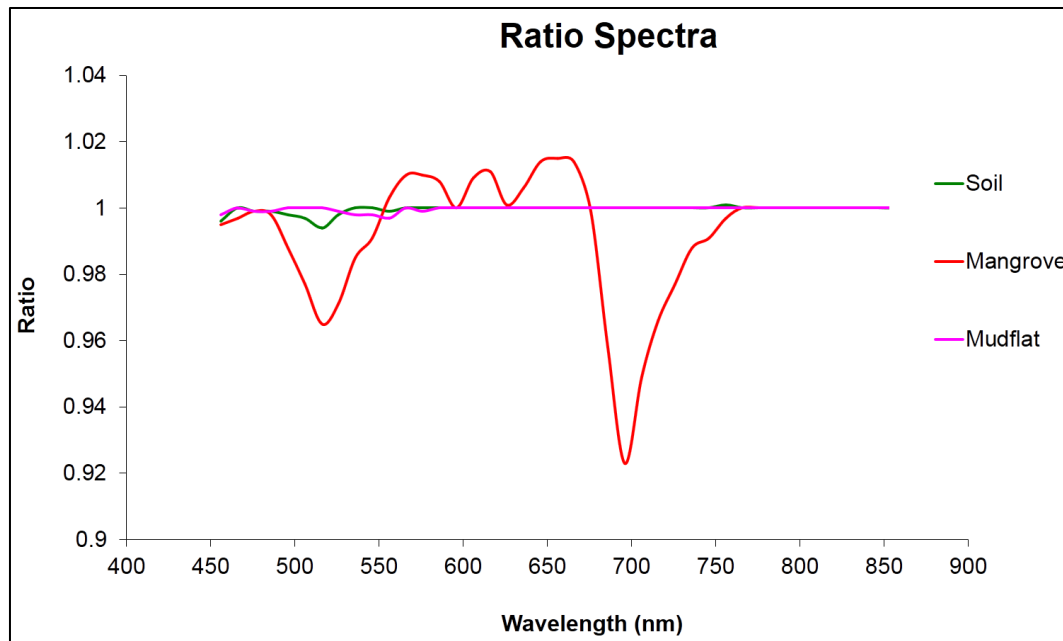


Figure 2.15: Ratio spectra obtained from ratio of original band and shifted band

2.3.2 Understanding the issues in vegetation spectra

The typical vegetation spectra, shown in textbooks, are of the type shown in figure 2.7. In reality, the spectra obtained for vegetation through airborne and spaceborne missions have many issues, especially with regards to range of values, that need to be understood. Apart from giving the necessary information about the phenological state, vigor, health etc. of the vegetation, study of vegetation spectra serves an important purpose of checking the response of the hyperspectral instrument. This feature is illustrated in this section.

The remote sensing images are generally provided in Digital Numbers (DN) which are converted to radiance units by using the saturation radiance or gain setting of the instrument and the level of quantization (equation 1).

$$\text{Radiance} = (\text{DN}/\text{Quantization}) * (\text{L}_{\text{max}} - \text{L}_{\text{min}}) + \text{L}_{\text{min}} \dots \dots \dots (1)$$

where, L_{max} =Saturation Radiance, L_{min} = offset and quantization defines the radiometric resolution or the number of bits.

If needed, atmospheric correction is also done over the radiance images to yield images of actual and sometimes apparent reflectance. At both the radiance and reflectance levels, the range of values is of significance, as stated earlier and shown below.

2.3.2.1 Method

The spectral plots in radiance domain were taken for two kinds of vegetation-forests and agricultural crops. The pattern and magnitude of the spectra were analyzed for both the cases using AIMS data. Based on this analysis, inputs were provided at the processing level leading to improved AIMS version. The spectral plots in reflectance domain were then studied for forests and again scope for further refinement was suggested, which was duly done. Once, all the suggestions were ingested, spectral profiles for vegetation through AIMS data were compared with those of Hyperion. But, the issues with the range of values still existed, so, reflectance plots of three kinds of targets were compared using Spectroradiometer observations and AIMS data after folding Spectroradiometer observations to AIMS specifications for sufficing to one-to-one match. But, still some anomalies existed. So, an experiment was conducted in the clean room facility for checking AIMS observations with those of ASD Spectroradiometer at four known illumination levels. The radiance was recorded for both the instruments and deductions were made.

2.3.2.2 Results and Discussions

ROIs of 3 pixels by 3 pixels were taken from a class of dense forests and full cover crops of AIMS data. Mean radiance was computed for both the classes and is shown in Figure 2.16. Sharp gaseous absorption feature is observed at 762nm corresponding to Oxygen. Minor absorption features near 520nm, 690nm and 840nm were also observed. The features nearing 840nm are mainly owed to water vapor while 690nm corresponds to chlorophyll absorption. Despite this, the spectra do not resemble the typical vegetation spectra, especially because these are the spectra for dense vegetation which should have a small peak at 550nm and then high radiance in NIR region. Moreover, near 650nm, sharp dip in radiance value is seen which indicates some kind of fault with the sensor element or in the processing stage. Furthermore, huge out of band response is seen throughout the spectrum. This results in shielding or concealing of the relevant peaks and dips.

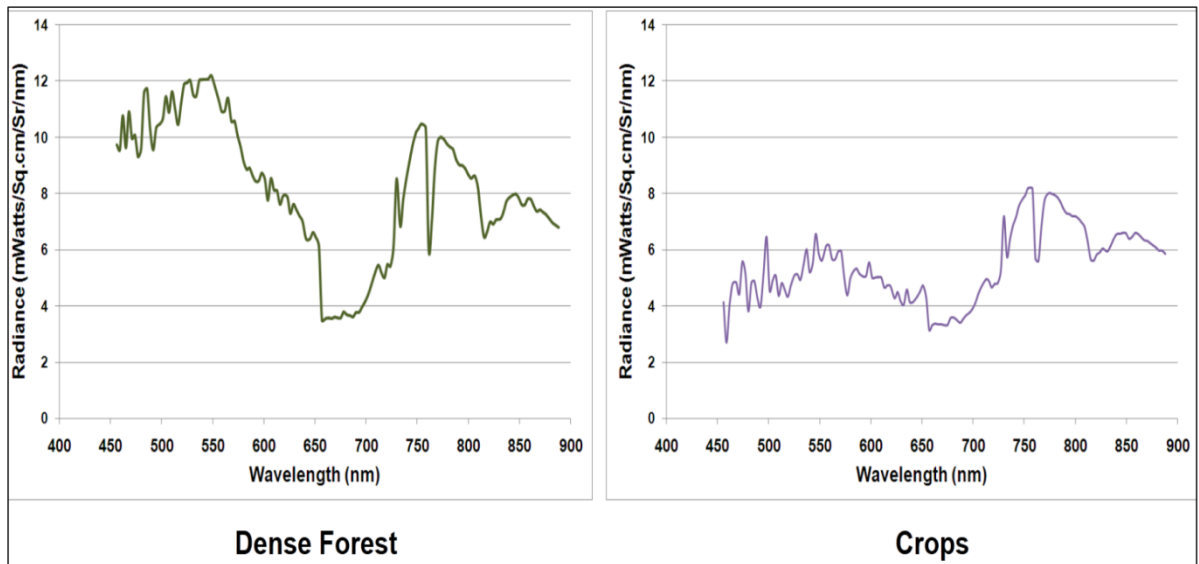


Figure 2.16: Radiance plots generated for vegetation using AIMS data

Post this analysis, AIMS data was rectified. So, again, the spectrum was taken for vegetation (figure 2.17).

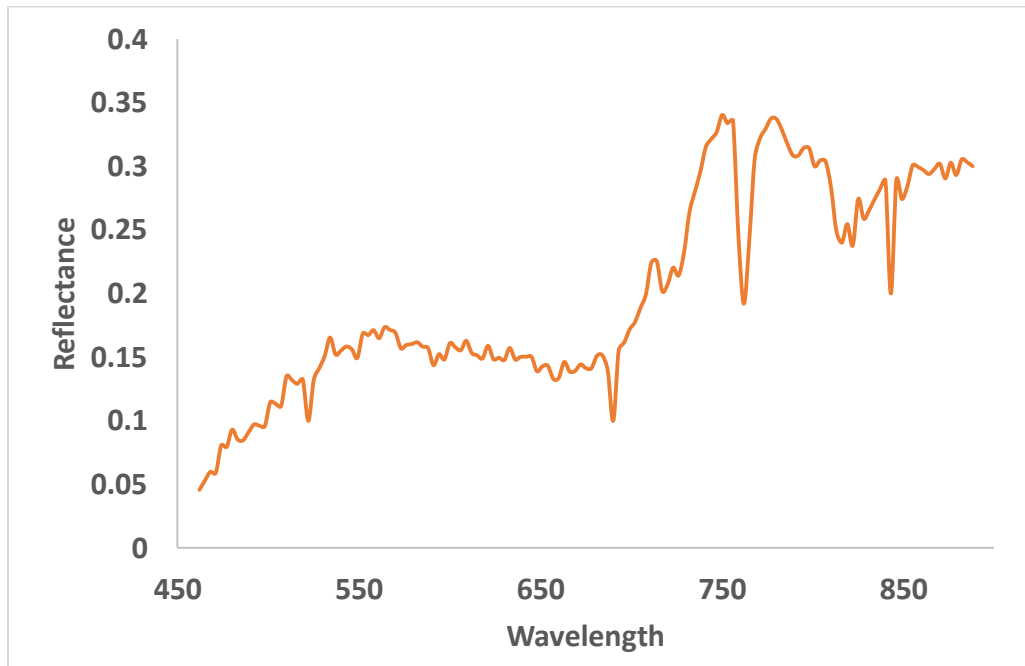


Figure 2.17: Reflectance plot for vegetation generated from AIMS data

The typical pattern of vegetation spectra is seen in this case- relatively high reflectance at 550nm in visible region and high reflectance in NIR range. But, there are certain issues as well which demand further action. These are: 1) This is a reflectance spectrum, but, still the dip nearing 762nm exists, which is not related to Oxygen absorption as this was an atmospherically corrected image. The same is true for other absorption regions, 2) The change in reflectance from visible to NIR is not sharp but rather subdued. This kind of feature is generally present in stressed vegetation. But, in this case the vegetation was

healthy, as confirmed from the ground observations, 3) The spectra exhibited huge out of band response. Due to which, the characteristic absorption features as well as the corresponding range of reflectance values are difficult to interpret. This is shielding the characteristic absorption features of many molecules including water. All of these factors imply that AIMS data needed further refinement.

After further refinement in the data, the spectra were then taken for Mangroves, fallow land and mudflat and are shown in figure 2.18. Also shown are the spectra for the same classes from Hyperion data. Irrespective of the class and slight smoothing, AIMS spectra showed two unique yet prominent features between 500 and 550nm. These features are systematic for every target in the scene and do not owe their presence to any commonly known target. This implies the presence of significant problem with the data that has to be handled at payload or at the processing end. Moreover, the range of data values does not match at all. The radiance values for Mangroves are relatively higher ($\sim 6 \text{ mW/cm}^2/\text{sr}/\mu\text{m}$) than other targets in NIR region, but still less than what is expected from high biomass and rich chlorophyll regions. For e.g., in case of grain formation stage of Sorghum, a case of high biomass and chlorophyll, radiance values reached nearly $10 \text{ mW/cm}^2/\text{sr}/\mu\text{m}$ when HySI data was used (Kumar, 2010) and also for Mangroves, the radiance value in NIR region reached up to $10 \text{ mW/cm}^2/\text{sr}/\mu\text{m}$ when Hyperion data is considered (Panigrahy et al., 2011).

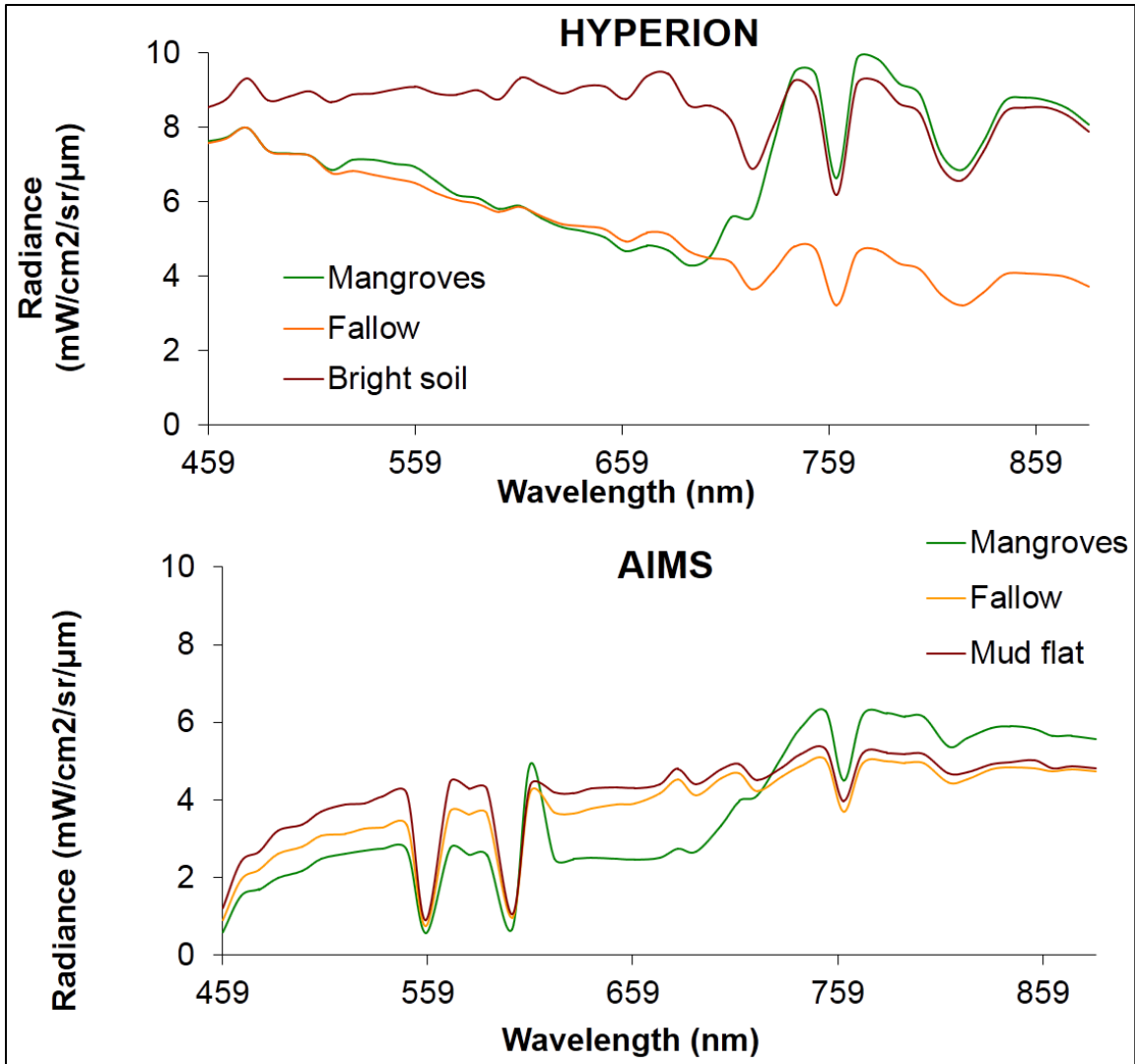


Figure 2.18: Radiance plots for vegetation using AIMS data and the corresponding areas Hyperion data

Now, it was clear that the data needed further check or refinement as it did not match well with the values cited in literature. So, hand-held Spectroradiometer measurements were taken to analyze AIMS data. Since, Spectroradiometer specifications were different

from those of AIMS, Spectroradiometer specifications were simulated to match with AIMS and then the observations were plotted (shown in figure 2.19).

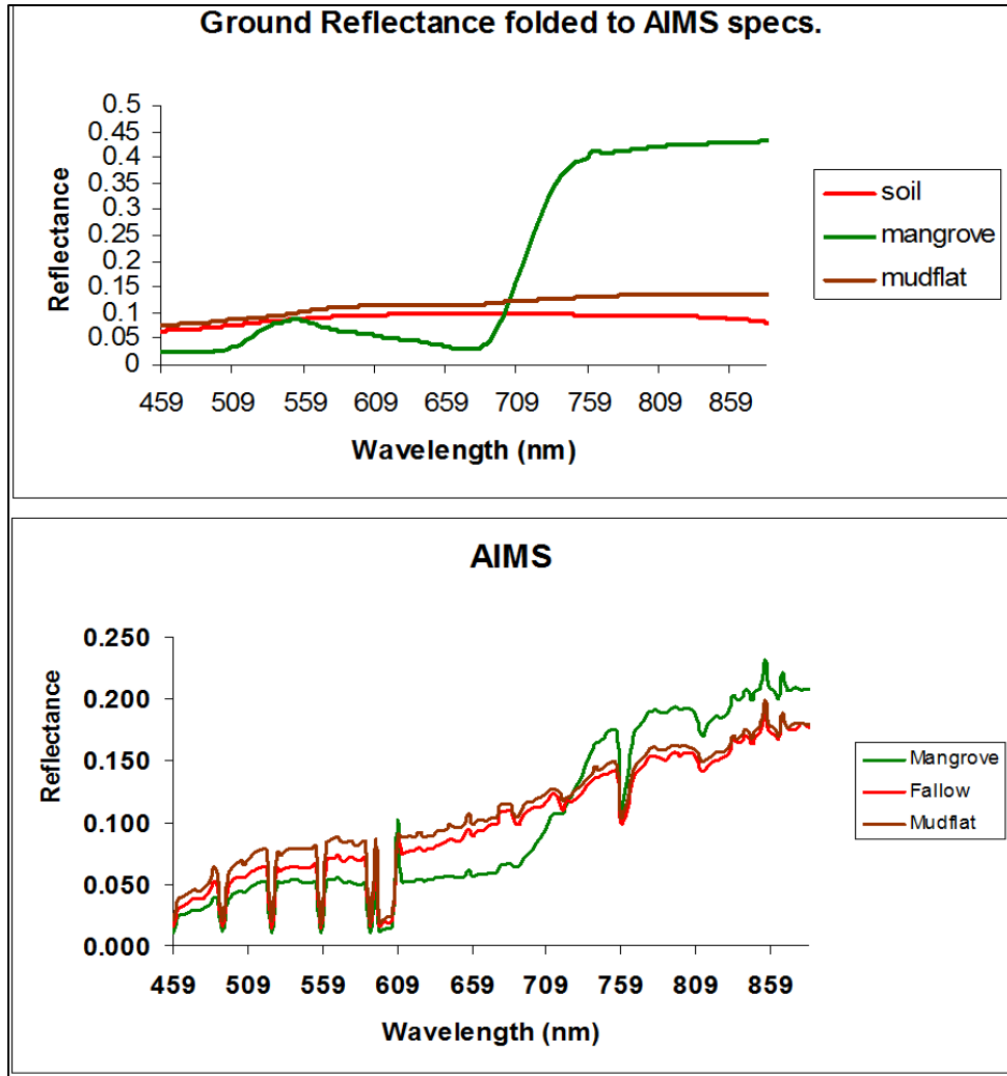


Figure 2.19: Reflectance plots for AIMS data and from hand-held Spectroradiometer data folded to AIMS specifications

The reflectance plots of AIMS from the figure show that even after atmospheric correction, out of band response could not be corrected. Moreover, the unexplained

strong absorption points found earlier still exist, in addition to a few more. In view of these issues, it was decided to examine the AIMS instrument with hand-held Spectroradiometer in the laboratory at known illumination levels.

Thus, an experiment was conducted in the clean room facility for checking AIMS observations with those of ASD Spectroradiometer at four illumination levels. The radiance was recorded for both the instruments (Figure 2.20). Corresponding difference in radiance measured by the two instruments is shown in figure 2.21.

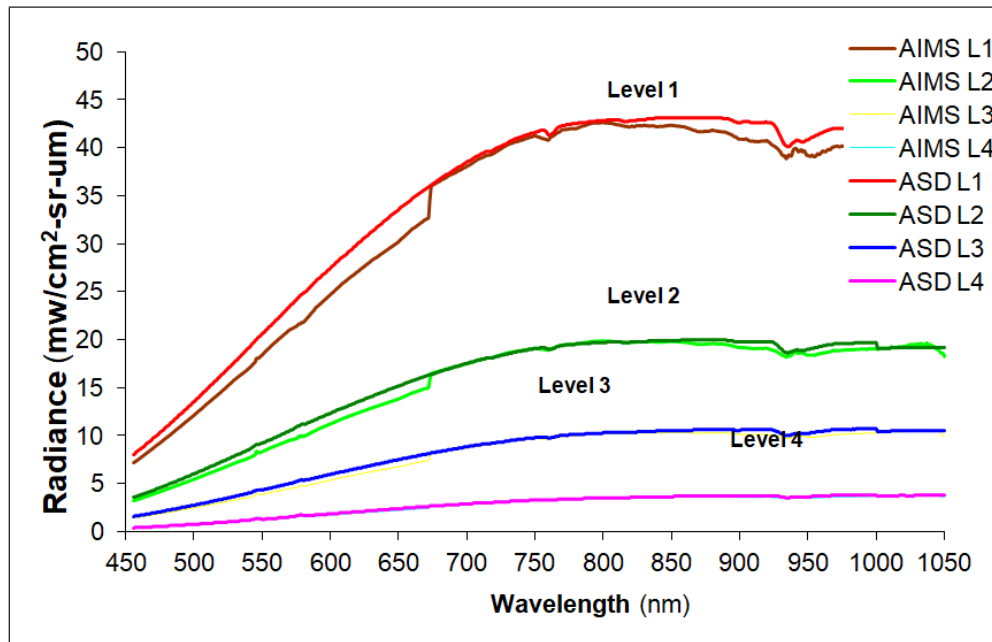


Figure 2.20: Radiance (mw/cm²-sr-um) measured in Lab by AIMS & ASD Spectroradiometer at different lighting level

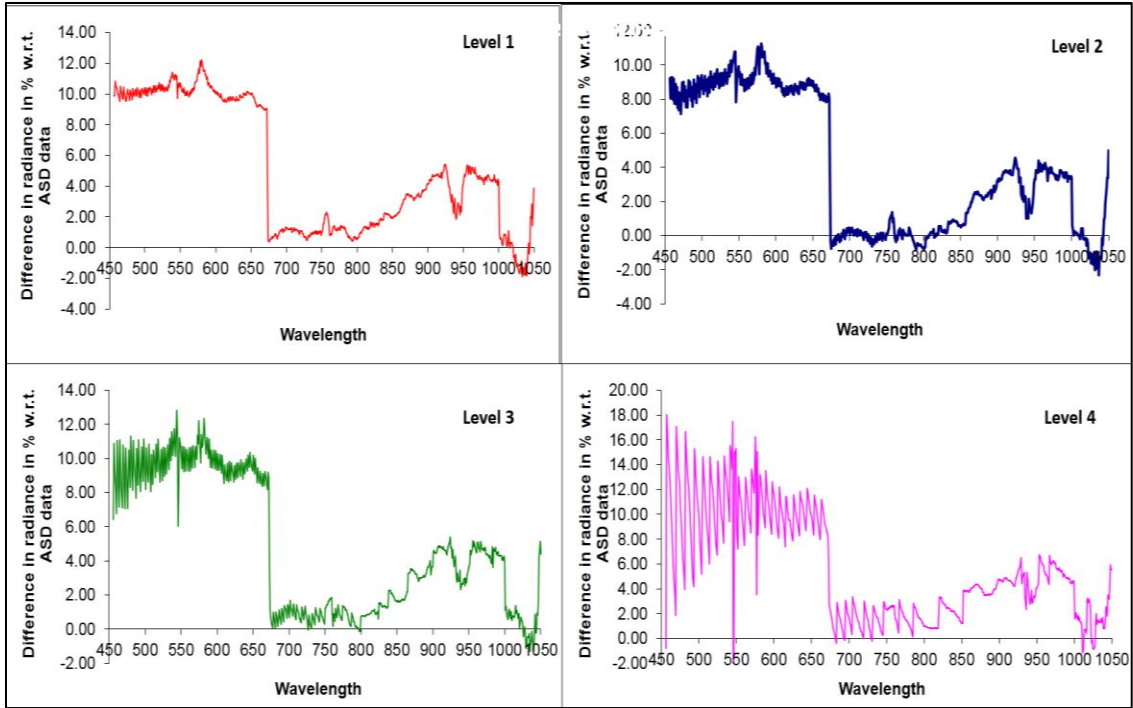


Figure 2.21: Difference in Radiance measured between AIMS & ASD Spectroradiometer at different lighting levels

From the above figures, following inference were made-1) Radiance values measured by AIMS and ASD Spectroradiometer were of similar order, 2) AIMS radiance values were lower than ASD by 8-12% in visible bands (up to 673 nm), later on the values were within 5% of ASD, 3) There is small jump in radiance of AIMS around 673 nm.

Thus, all of these analysis, mainly based upon vegetation spectra, bought clarity to the observations and gave an insight on creating correction coefficients for AIMS data.

2.3.3 Band-to-band registration

Many times, due to the aircraft/spacecraft jitter and/or due to scanning mechanism, the hyperspectral sensors suffer from band-to-band mis-registration. Sometimes, it is visible

through the naked eye, sometimes on zooming and sometimes it is difficult to find on visual inspection. The three cases are shown in figure 2.22. Out of these three cases, the most troublesome is the third case because in such cases the user is under the impression of perfect registration but on doing quantitative analysis and/or geotagging, the unexpected results arrive.

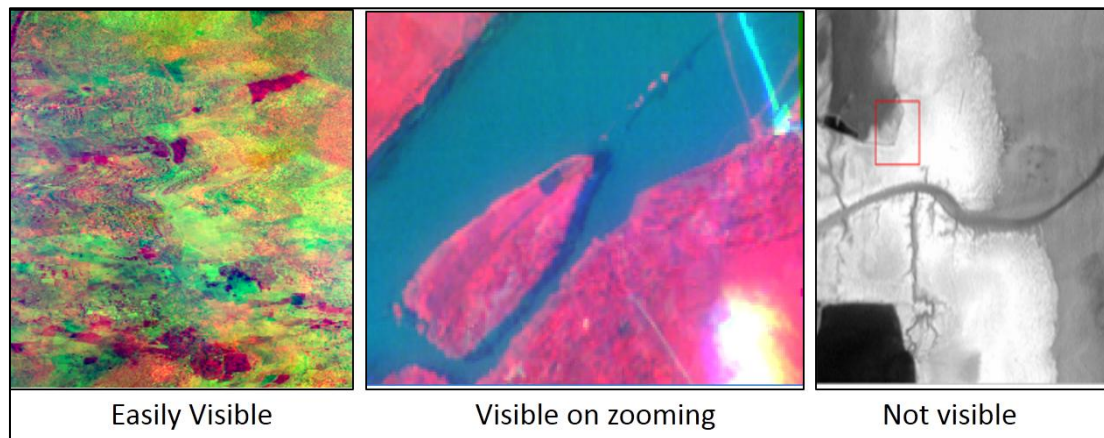


Figure 2.22: Band-to-band registration seen at different zooming levels in different images

Thus, in addition to qualitative assessment of band-to-band registration, quantitative analysis is also necessary.

2.3.3.1 Method

Band-to-band registration can be checked through two means-qualitative as well as quantitative. For qualitative check, a number of bands, spread across the spectrum, were randomly selected. These bands were then linked together for visual inspection using ENVI image processing software. Change in position of the cursor in one band leads to

the same location in all other bands displayed, confirms good band-to-band registration. So, a number of ROIs were selected, whose position shift is easily conceivable like sharp features involving road crossing, curves etc. For quantitative assessment, a large number of Ground Control Points (GCPs), analogous to ROIs mentioned above were taken. Root Mean Square Error (RMSE) was computed for each. A lower RMSE value signifies correct band to band registration, preferably below 0.3 pixels (Wang et al., 2013; Jiang et al., 2013). Furthermore, to understand its implication on vegetation assessment, a classified image of mangroves was discussed.

2.3.3.2 Results and Discussions

Sometimes band-to-band registration is too poor such that it is visible clearly like in Figures 2.23 and 2.24 representing two sets of AHySI data.

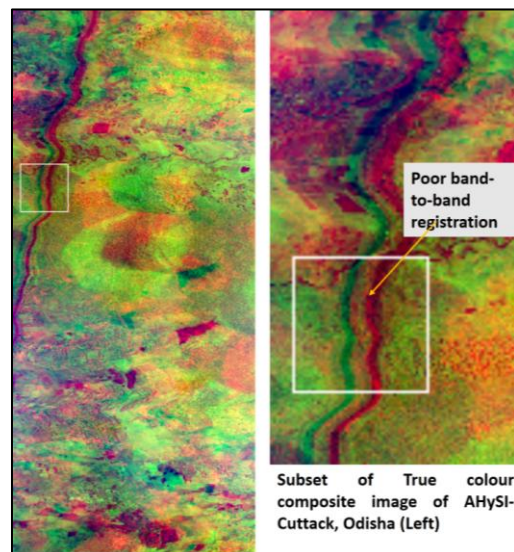


Figure 2.23: AHySI data showing poor band-to-band registration along with lots of

noise

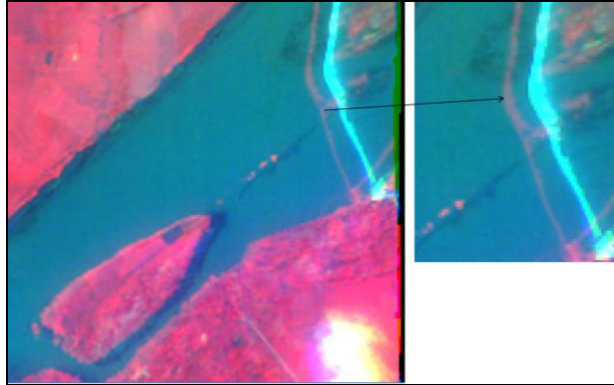


Figure 2.24: AHySI data showing poor band-to-band registration

But, many a times, band-to-band mis-registration is not visible from the naked eye. For such cases, quantitative assessment has to be done. To demonstrate this idea, AIMS data was selected. Qualitative assessment was done by selecting evenly spaced bands (total seven in number) and shown in figure 2.25. In the figure, region enclosed in red box shows the same area (a typical sharp curve) in different bands from AIMS data. This qualitatively shows a good band-to-band registration.

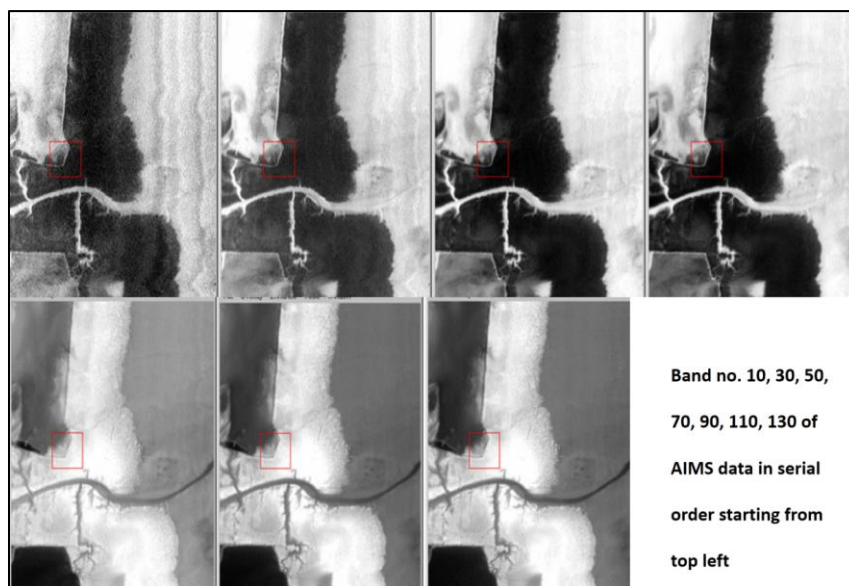


Figure 2.25: Different bands representing same locations for AIMS data

For quantitative assessment, a total of 15 GCPs were taken. Care was taken in selecting the GCPs such that they should exist on the sharp curves or intersections so as to pinpoint their location. Table 2.8 gives RMSE for different bands w. r. t. band 100. The choice of band 100 is based upon the fact that it lies at the middle of the spectral region and so is assumed to be free from calibration and noise issues.

Table 2.8: RMSE values for GCPs

Band no.	RMSE for Jamnagar
20	0.2
30	0.3
40	0.2
50	0.7
60	0.4
70	0.4
80	0.4
90	0.4
100	0.5
110	0.5
120	0.5
130	0.5
140	0.5

The results from the above table imply that although the images look perfect, the band-to-band mis-registration may exist. In this case, RMSE varied from 0.2 to 0.7, which is outside the acceptable range given by Wang et al. (2013) and Jiang et al. (2014). Thus, a *quantitative check is a necessary requirement for checking band-to-band registration*

before further analysis. Its implication on vegetation assessment can be understood from the following example, shown in figure 2.26. This figure shows classified image having pockets of mangrove species. There are certain regions (circled in red colour) which show two classes occurring together or are adjacent to each other. These are the classes where the effect of band-to-band mis-registration is most pronounced because in such cases when the two species are adjacent and if this issue exists, the pixel may be wrongly classified.

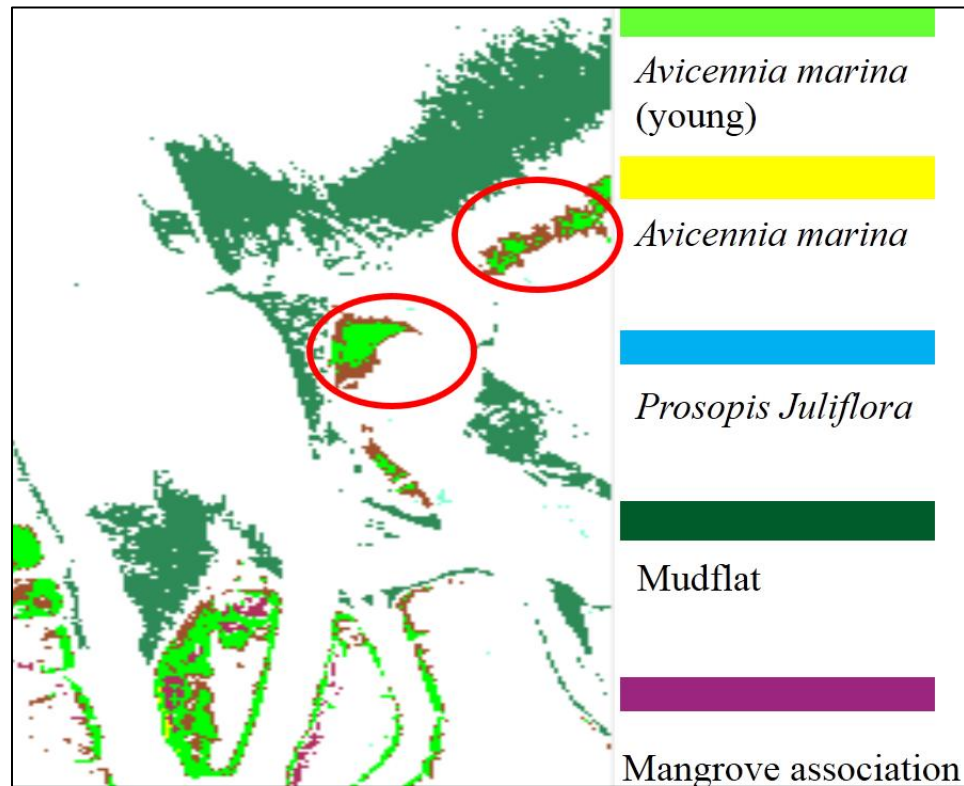


Figure 2.26: Classified image of Jamnagar mangroves using AIMS data. Adjacent classes which may be affected by band-to-band mis-registration shown in red circles

2.3.4 Noise

Determination of noise through an image is difficult although in extreme cases it is easily visible, like in figure 2.27 wherein lots of stripes are seen. In the Hyperion imagery, all of these stripe artifacts are of one-pixel width (Yokoya et al., 2012). Noise due to striping deteriorates smile and keystone detection results. When the noise is apparent from the images but it becomes difficult to understand which bands to screen, one needs a quantitative assessment.

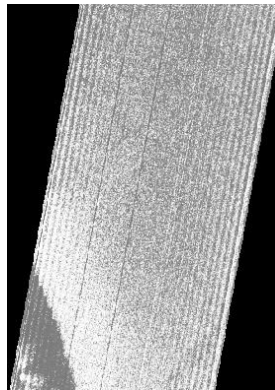


Figure 2.27: Hyperion image showing stripes

2.3.4.1 Method

Quantitative assessment of noise can be done through the computation of scene's Signal to Noise Ratio (SNR). To compute SNR, mean and standard deviation are taken for each pixel, which takes into account the neighbouring eight pixels in a window of size 3*3 pixels each. This is required to classify bad bands to be excluded from further analysis, using the following equation:

$$\text{Scene SNR} = (\text{mean of } 3 \times 3 \text{ pixel window}) / (\text{S.D. of } 3 \times 3 \text{ pixel window}) \dots \dots \dots (2)$$

where, S.D. is standard Deviation

As is evident from the formula, higher the S.D., lower is the scene SNR, indicating high scene noise. Bands having SNR <5 are removed from the analysis because such bands imply large noise (Rose, 1973).

2.3.4.2 Results and Discussions

Images from bands no. 1,5, 10, 15, 20, 25, 30, 60, 100 and 143 of AIMS are displayed in figure 2.28. Many bands in the AIMS scenes have moderate to high noise rendering some of them to be of limited use when further application is concerned. The initial few bands look noisy and hence can be easily removed, but later, noise does appear in some of the images. At this point, it becomes difficult to know where to put the threshold. In such cases, *computation of scene SNR becomes important.*

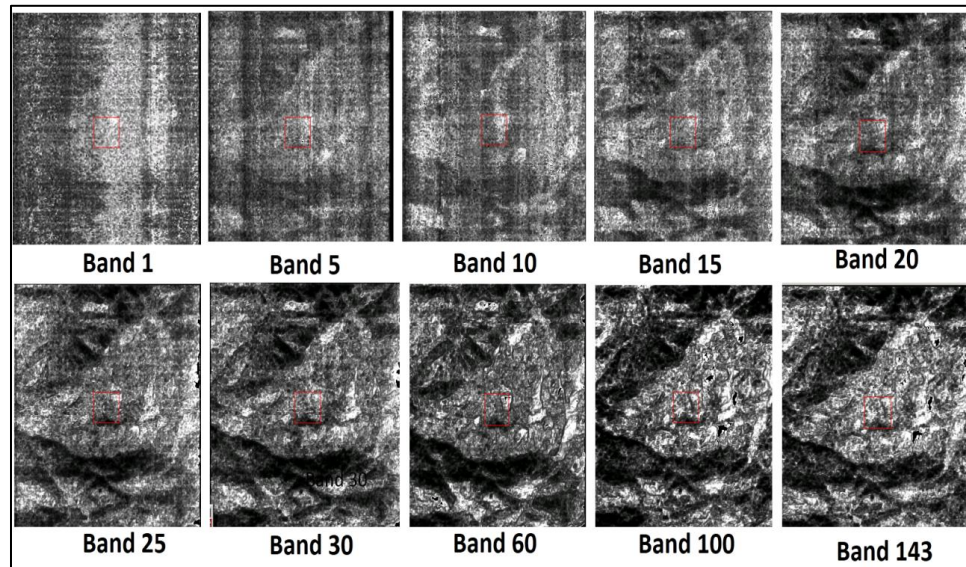


Figure 2.28: Randomly selected AIMS bands spread across the entire range

Using equation 2, scene SNR was computed for all the bands. The SNR w.r.t. band numbers is plotted in figure 2.29 for the scenes corresponding to figure 2.28 above.

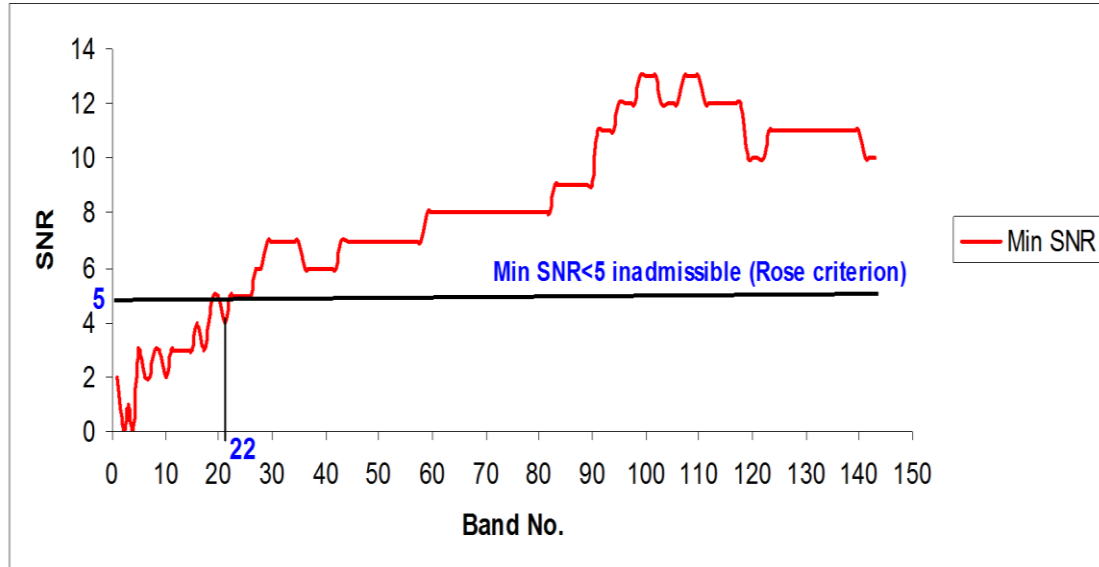


Figure 2.29: SNR value for AIMS bands. 1st 22 bands noisy.

Following Rose criterion, a total of 22 bands were removed. The influence of this was observed through vegetation classification. With all bands included, classification accuracy came out to be 62% which increased to 79% with the low SNR bands removed. Thus, *removal of noisy bands ups the classification accuracy.*

2.3.5 Image distortion

There are certain issues that are specific to airborne imaging. For e.g. Geo-referencing accuracy. Due to problems in synchronization between the navigation system and the sensors, sometimes small timing errors may occur causing scan lines to be positioned

incorrectly leading to development of "wobbles" in the imagery (<http://arsf-dan.nerc.ac.uk/trac/wiki/Reports>). This can be seen through figure 2.30.

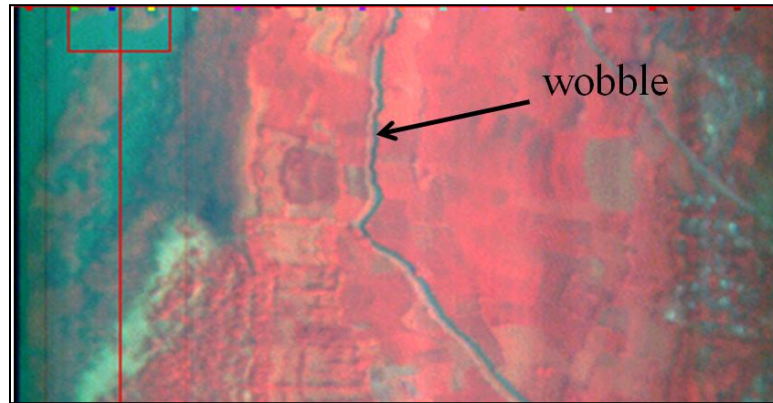


Figure 2.30: Wobbles in airborne hyperspectral imagery

2.4 SOURCES OF EXPERIMENTAL ERRORS THAT AFFECT DATA QUALITY

Even if the instrument is well calibrated and of scientific quality, yet it can offer poor quality end products due to human induced experimental errors. The errors induced at the time of data acquisition seriously affect the end products. Such factors are discussed in the following text.

2.4.1 Effect of change in exposure time

Exposure time refers to the time for which the scene on ground is exposed to the sensor. If the exposure time is high, it leads to blurring of the image. On the other hand, low exposure time causes low SNR (Janschek & Tchernykh, 2001). Therefore, while

acquiring hyperspectral images through AIMS data over a piece of land having agricultural crop field, forest, fallow land and water body (figure 2.31), acquisition time was set to 5ms and 10ms. For the ROIs representing targets of concern, shown in the figure below, mean radiance was computed, corresponding to which spectral plots were generated in radiance domain. These spectra were then analyzed.

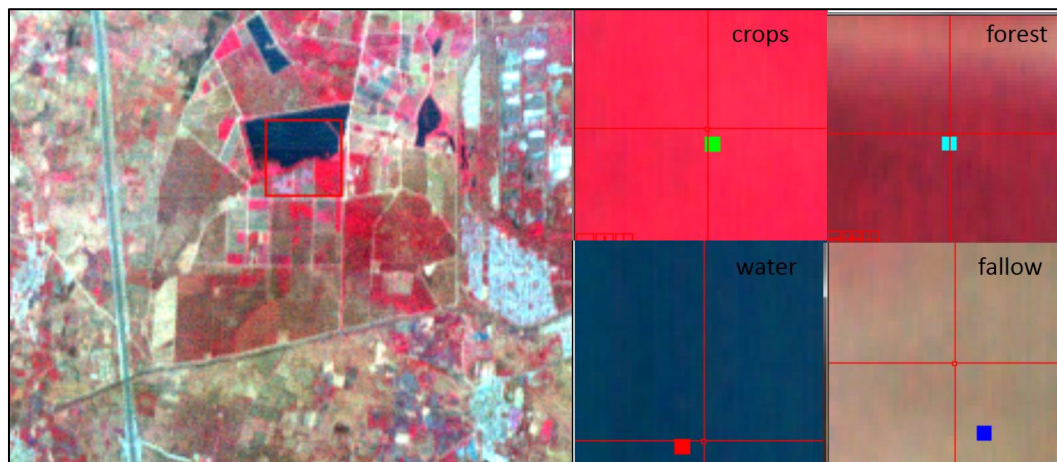


Figure 2.31: Target areas shown in AIMS image for which radiance is collected at two exposure times

2.4.1.1 Results and Discussions

There is a trade-off between the duration of the exposure time. Longer exposure time allows more light to enter the camera thereby increases the luminance of the image while a prolonged exposure leads to image blurring due to the movement of the objects. At two exposure times of 5ms and 10ms, the spectral analysis leads to some fixing facts. Figure 2.32 shows the radiance profile of the targets of interest shown in figure 2.31 at two

exposure times. At lower exposure times, the typical curves of the targets of interest are not observed. Also, the radiance values are subdued. However, with increase in exposure time, the magnitude of radiance values is increased but show a little higher range than normal. The pattern of the spectral profiles looks to be fine, apart from the out of band response. Overall, it may be said that *exposure time of 10ms is better than 5ms*.

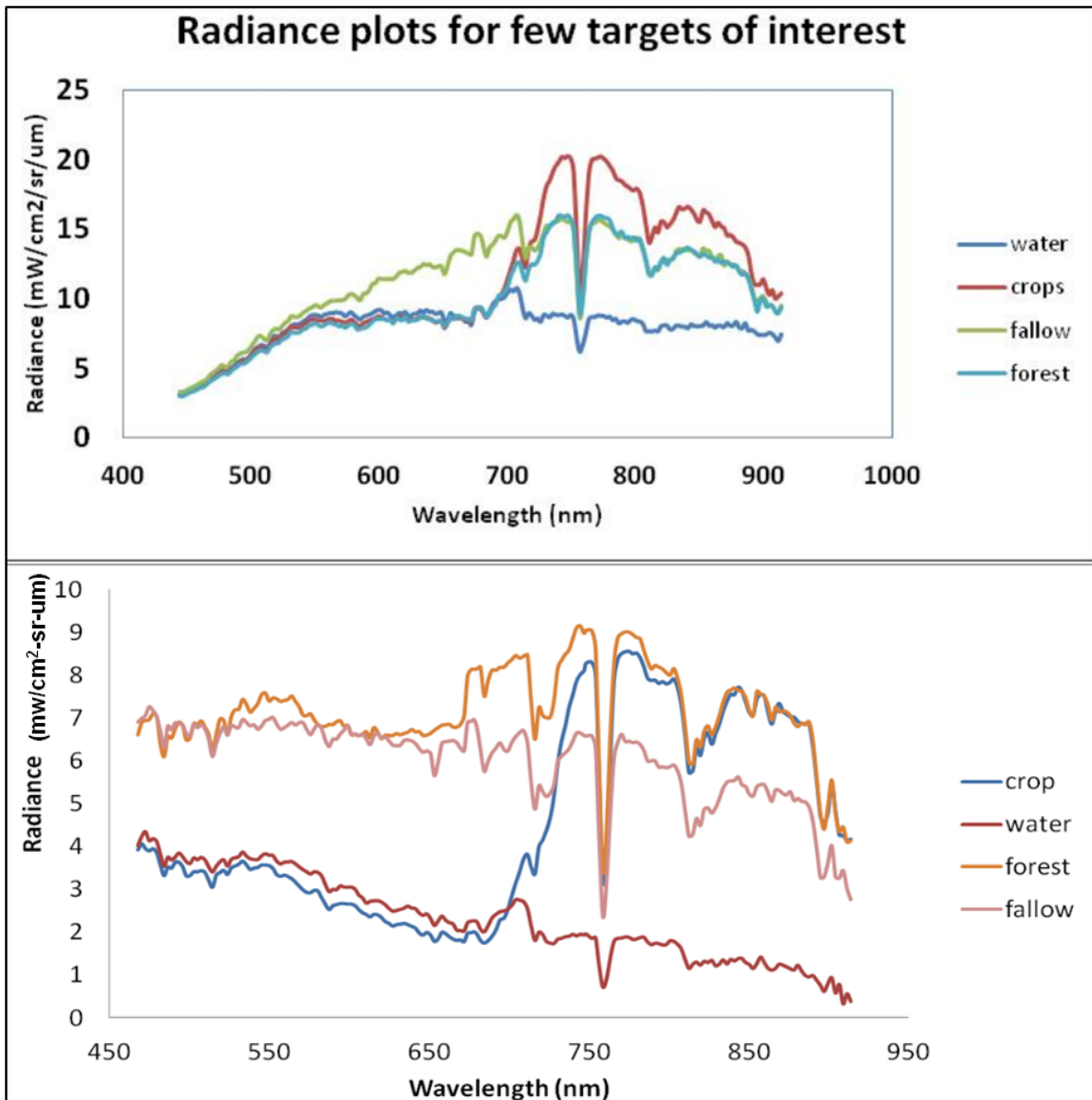


Figure 2.32: Radiance plots for targets of interest (shown in figure 2.31) at different exposure times-10ms (above), 5ms (below)

2.4.2 Effect of inappropriate sampling

Field Spectroradiometers generally measure a much smaller area, therefore, sampling complete area of interest becomes difficult. So, appropriate sampling strategy should be adopted. Even otherwise, when spectra are retrieved from the image, appropriate sampling

is necessary. One study suggests 10 samples is a good number (<https://discover.asdi.com>). The effect of sampling can be seen from figure 2.33. In this figure, three reflectance spectra, collected from hand-held Spectroradiometer, are shown for *Vigna unguiculata* (Cow pea). The spectra are obtained for three categories-1) when the number of samples is 5 and 2) when the number of samples is 7 and 3) for samples 10.

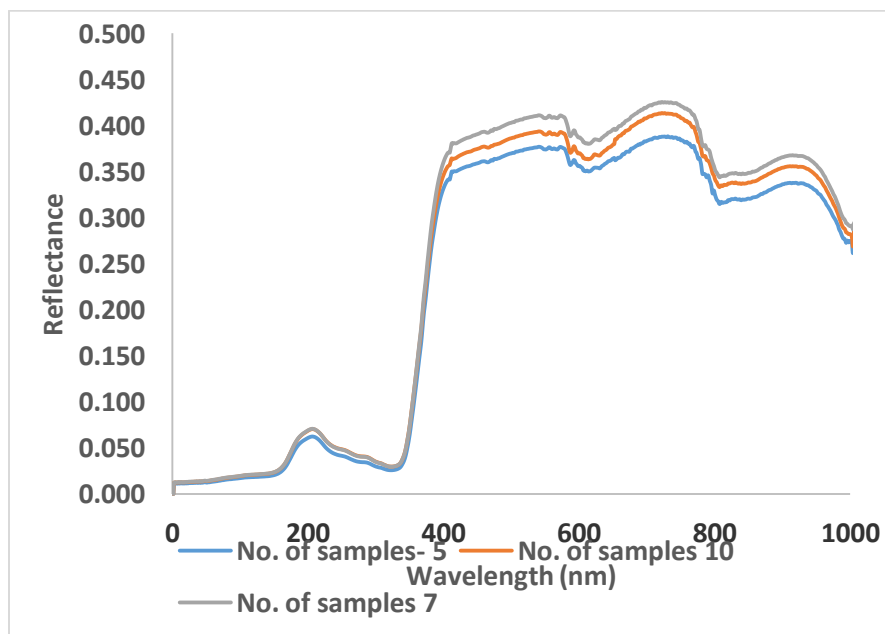


Figure 2.33: Effect of reducing number of samples on spectral behavior of *Vigna unguiculata* (Cow pea)

As can be seen from the figure, with the increase in number of samples, the diversity within the field is addressed well. Thus, the magnitude of the spectra changed substantially especially in the NIR region. Beyond 10 samples, the change in spectra is insignificant and is not shown in the plot. For quantitative estimates, percentage difference in the spectra is estimated. The same is shown through figure 2.34.

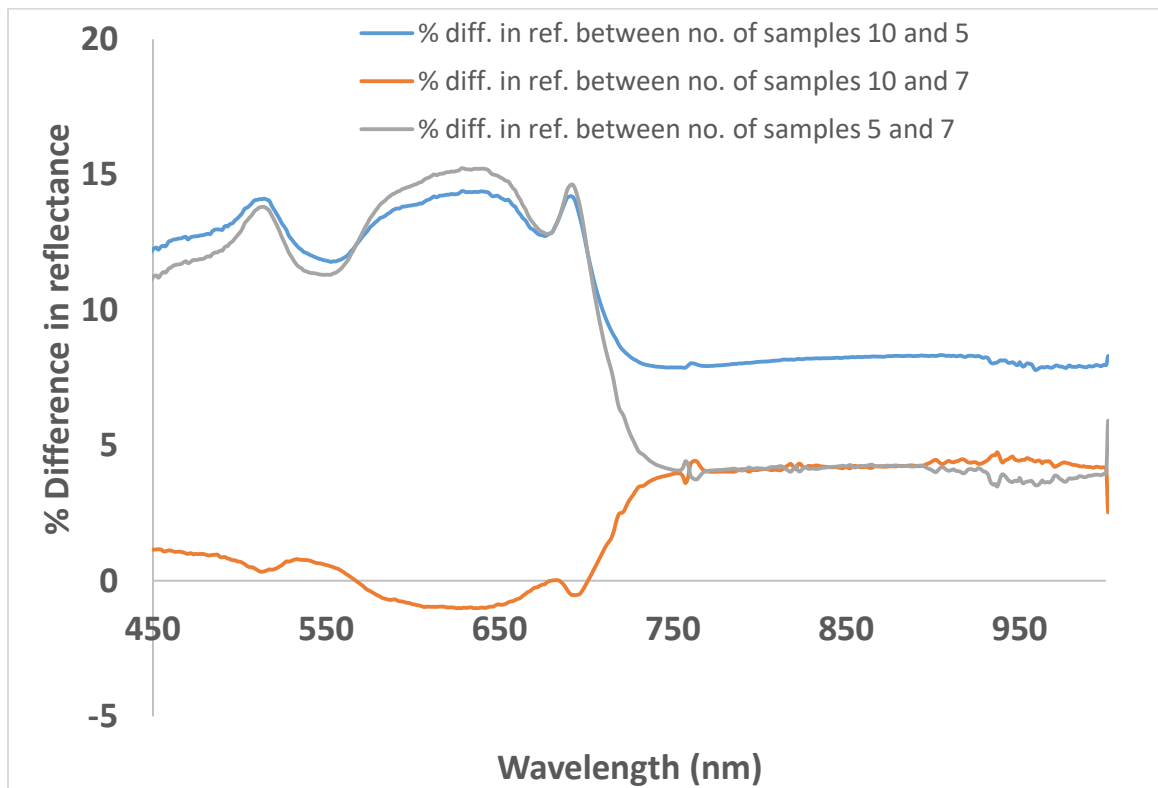


Figure 2.34: % difference in reflectance with change in number of samples

From the figure, it is seen that a difference of the order of 10-15% is observed within the visible range for sample size 5 and 7 or 10. Not much difference is observed between sample no. 7 and 10.

2.4.3 Effect of leaf stacking

When vegetation is mapped from the space or from any airborne platform, the effect of canopy as a whole comes. This includes several stacks of leaves, branches, flowers etc. It is expected that stack of leaves should increase the magnitude of the reflectance. So, spectral observations of leaves in stack of 1,2,3,4,5,6,7 and 8 leaves were taken. Figure 2.35 shows the spectral plots for a single leaf, two and seven leaves stacked of *Tectona grandis* (Teak).

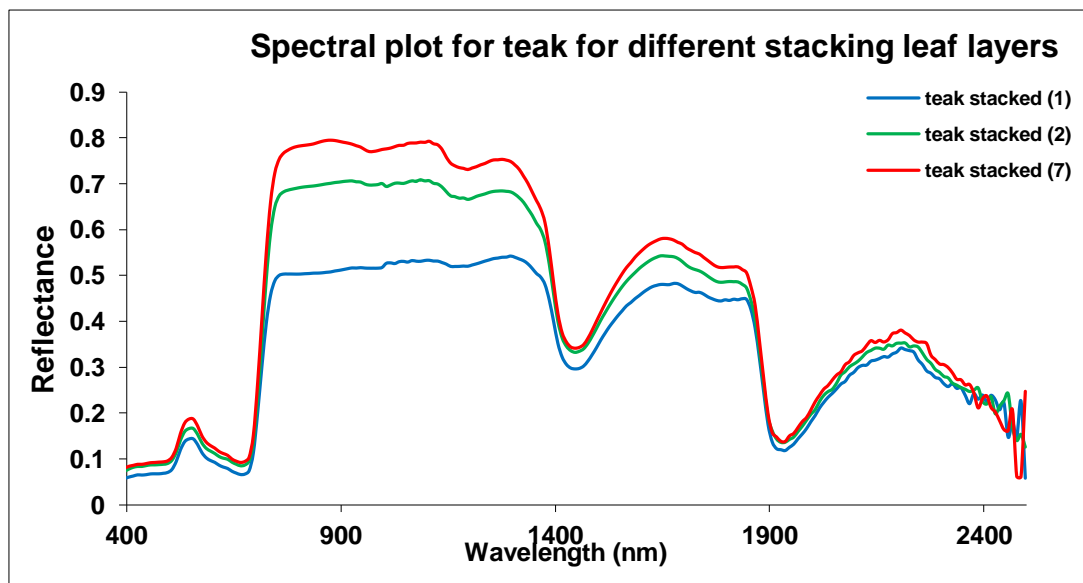


Figure 2.35: Effect of leaf stacking on spectral response of *Tectona grandis* (Teak)

As was expected, as the number of leaves in a stack increases, the magnitude of the spectra increases. This may create confusion in identifying two spectra. For e.g. a dense spectra of one vegetation may mimic less dense spectra of another. Thus, associated ground information is also necessary while labelling the target vegetation in the image. The extent to which the reflectance varies can be seen from figure 2.36.

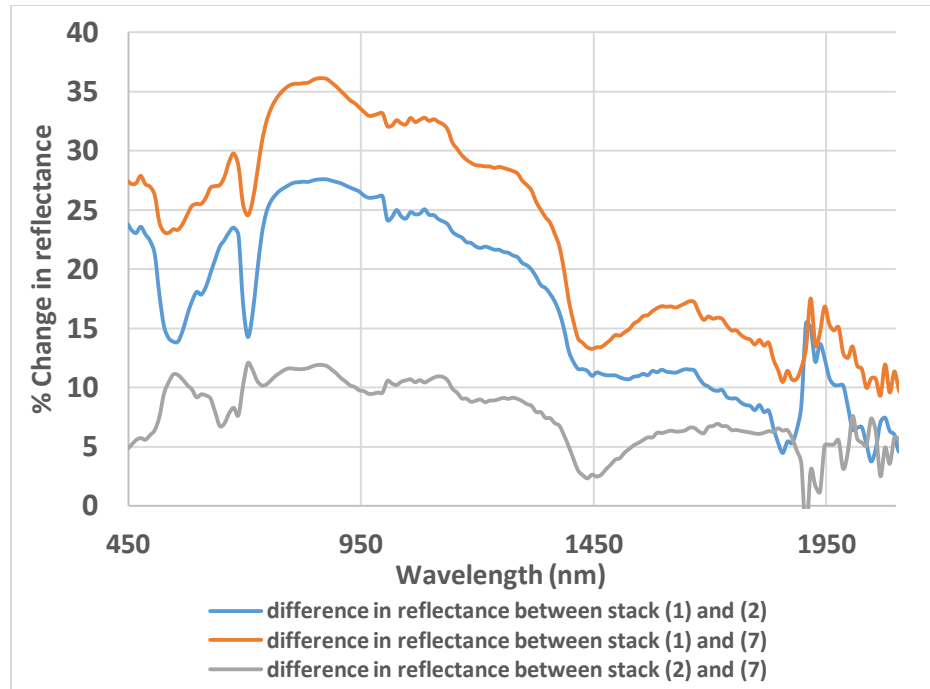


Figure 2.36: % Change in reflectance with leaf stack

As soon as the number of leaves change from 1 to 2 in a stack, the reflectance increases and it keeps on increasing with the increased number of leaves in a stack. However, the change in reflectance is comparatively low between a stack of 2 leaves and 7. Thus, it may be concluded that *reflectance of single leaf does not give the actual picture of the canopy but a stack of even two leaves is better.*

2.4.4 Effect of phenology

Phenology refers to timing of life cycle events of a vegetation especially w.r.t. changes in season. This means phenology of vegetation includes all the life stages of vegetation including sapling, fruiting, mature age etc. At each level, the constituting pigments also vary in proportion. To understand this clearly, two cases are considered-for tropical tree

species *Madhuca indica* and *Tectona grandis*. For *Madhuca indica*, spectra for two stages are plotted in figure 2.37- for very young leaf and for mature leaf. Since the pigment composition, leaf's surface properties, structure and water content of young leaf and mature leaf vary greatly (Croft and Chen, 2017), the spectra of the two leaf types also vary. The spectral plot for the mature leaf is the standard one and is usually found on ground as well as in spectral library. The spectrum of young leaf does not resemble the typical reflectance curve for vegetation. If this signature is used for training purpose, the resulting classification would be erroneous. This is an example where spectra interpretation can introduce huge conflict. Thus, knowledge of phenological stage of the vegetation is of utmost importance before using the spectra for further analysis.

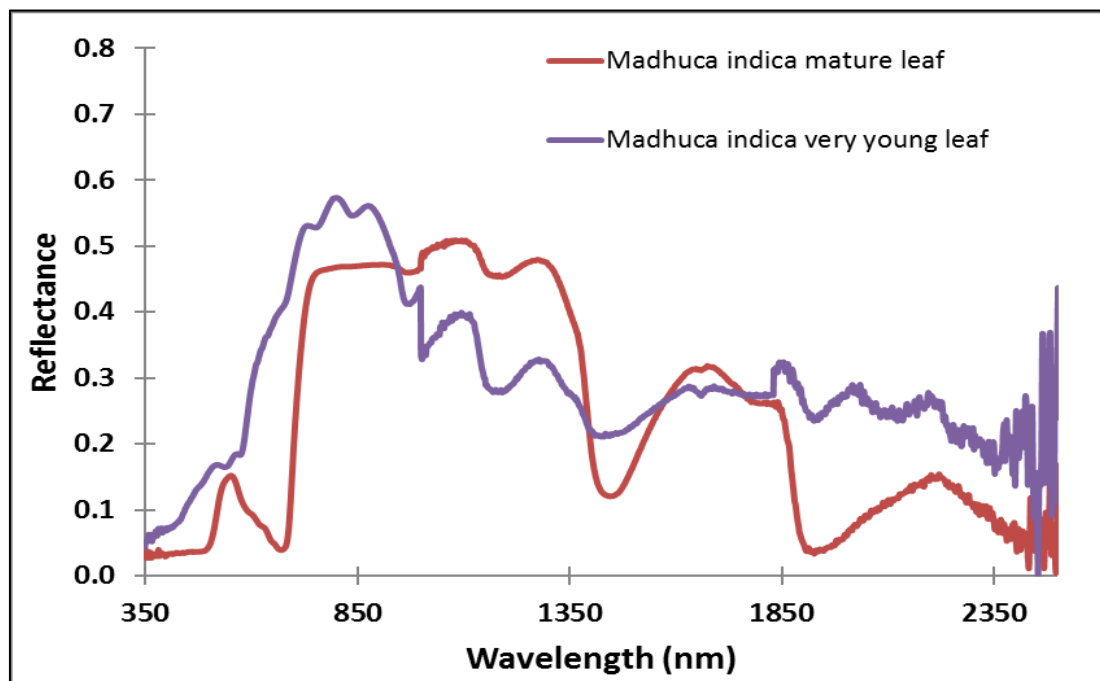


Figure 2.37: Spectral plots of the two growth stages of *Madhuca indica*

In another example, various stages of *Tectona grandis* (Teak) starting from young age to mature age is taken. The spectra of the same is plotted in figure 2.38.

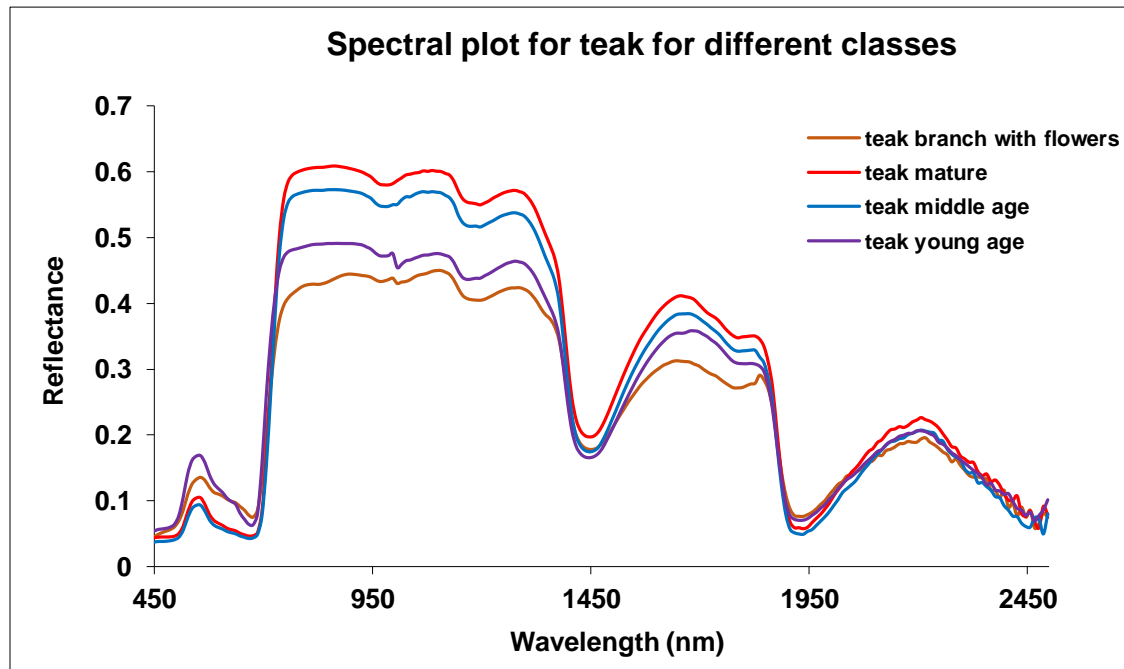


Figure 2.38: Phenological stages of *Tectona grandis* (Teak)

Here, unlike the spectrum of *Madhuca indica*, the variations in spectra are mainly in magnitude and not the pattern (apart from a few variations).

From above, it may be concluded that *the phenological stage of the vegetation under study should be borne in mind before any deduction is made.*

2.4.5 Effect of variety

The variation in spectra owing to the change in species is shown by many researchers (Zhang et al., 2012; Singh et al., 2012; Jeffery et al., 2014). Within the same species also, the varieties may be different (Moharana & Dutta, 2014). To understand the range of variation of the reflectance within the same species, spectra from six different varieties of paddy were studied. The spectral plots are shown in figure 2.39. Here, three important observations are made: First, the spectral plots vary mostly in the NIR range, both in magnitude and the position of absorbing wavelengths, Second, the position of red edge changes with each variety and thirdly, the magnitude of green peak also varies with variety. Thus, the paddy varieties, which apparently look similar are easily distinguishable using hyperspectral remote sensing.

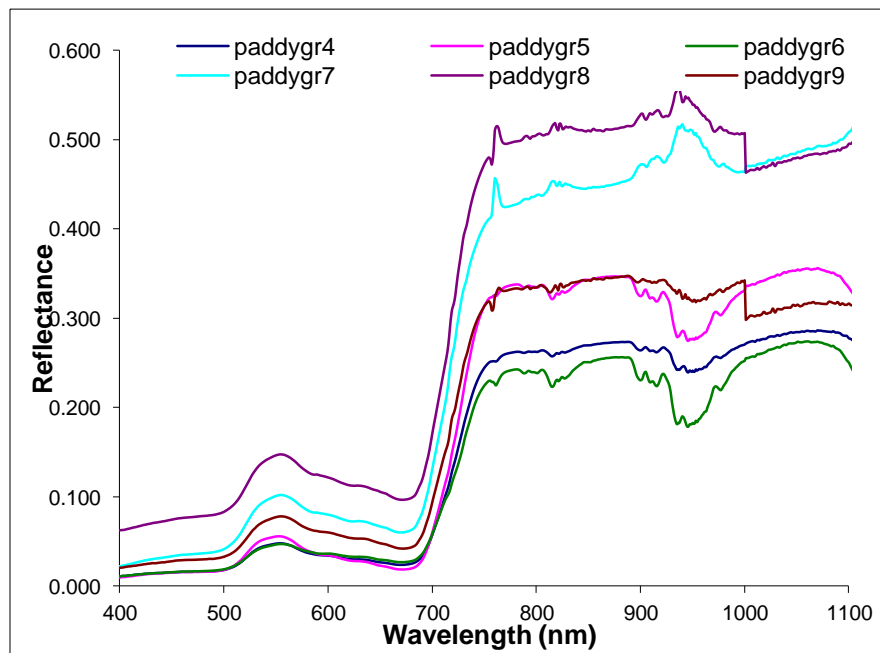


Figure 2.39: Spectral curves of various varieties of paddy crop obtained using ground based Spectroradiometer

2.4.6 Effect of sensor saturation radiance

Saturation Radiance (SR) is the radiance recorded by the sensor at saturation, which occurs when the energy flux exceeds the sensitivity range of the detector. It is an important parameter while designing the sensor. For a given quantization level, higher SR may lead to decrease in spectral discrimination while the lower SR may result in saturation over the desired area of interest. To understand the influence of sensor SR, let us take two cases for the three hyperspectral instruments whose SR is shown in figure 2.40.

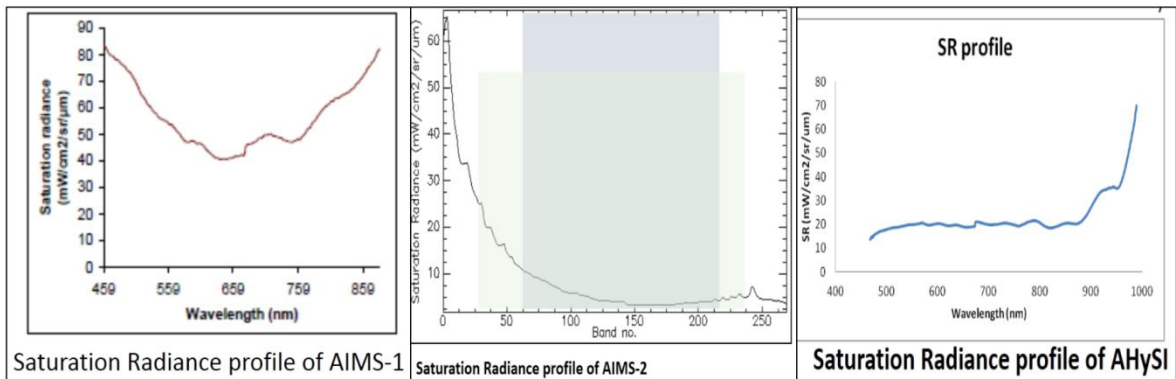


Figure 2.40: Saturation radiance plots for the three airborne sensors-AIMS-1, AIMS-2 and AHySI

Case 1 corresponds to radiance at 450nm from all of the three instruments when quantization is 8 bit and case 2 corresponds to the same calculations for 12-bit quantization. It is assumed that the target has $DN=100$.

Radiance can be computed from the standard equation (1) and assuming L_{min} to be 0.

Table 2.9 displays the calculated values for the two cases.

Table 2.9: Effect of SR on three airborne sensors

	AIMS-1 radiance	AIMS-2 radiance	AHySI radiance
Case 1	31.25	19.5	5.9
Case 2	1.95	1.22	0.37

No doubt, same DN value corresponds to variable radiance with change in SR. *Thus, the choice of SR plays a great role in obtaining the radiance for the target of concern.*

2.4.7 Species considerations

Different species vary in pigment composition and quantity (Kiang et al., 2007; Croft & Chen, 2017). As a result, they show variation in spectral behavior. Jeffrey et al. (2014) and Zhang et al. (2012) have showed role of various spectral regions in species discrimination from hyperspectral data. This can be understood from the spectral plots shown in figure 2.41 (for agricultural crops) and figure 2.42 (for mangrove tree species).

The spectral variations are seen both in magnitude and points of absorptions, especially in the VNIR regions and the red edge positions for both the agricultural crops and the mangrove species.

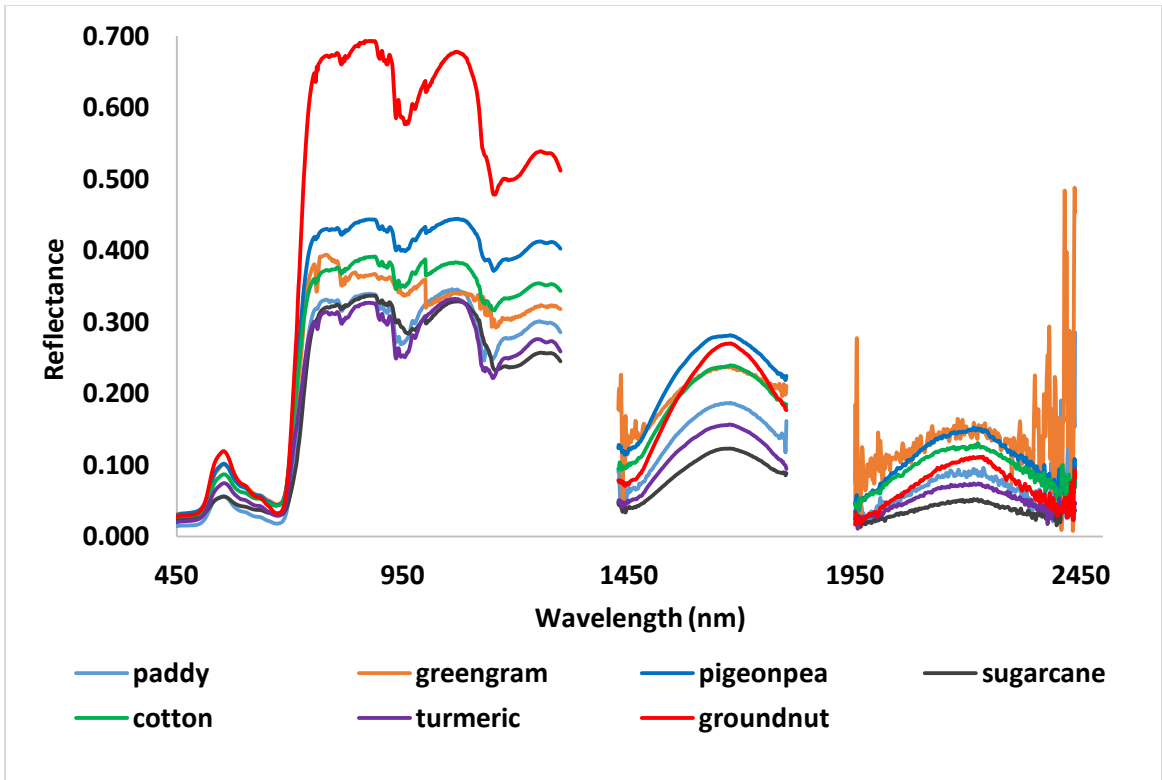


Figure 2.41: Spectral variations seen in typical reflectance spectra of agricultural crops

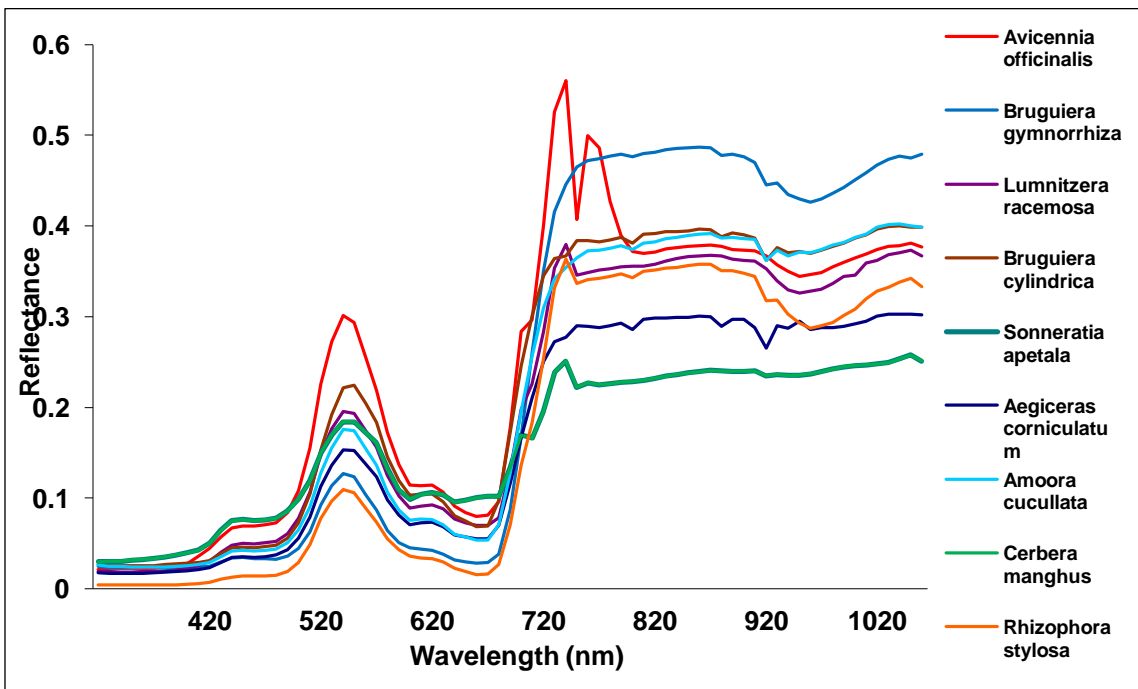


Figure 2.42: Spectral variations seen in typical reflectance spectra of Mangrove tree species

2.4.8 Others

Other factors that need to be addressed beforehand include:

- Field Spectroradiometers generally measure a much smaller area, therefore, sampling complete area of interest becomes difficult. So, appropriate sampling strategy has to be adopted.
- Many times, field measurements include scattered light from clothes of observer. It is thus advisable that the observer avoids bright cloths and keeps himself away from the camera's Field of View (FOV).
- For repeated observations, the hand may not remain still leading to changes in observations. Therefore, a well levelled tripod or stand is required.
- When using the instrument outside, reference spectra should be taken as soon as sun's angle change, atmospheric changes, like cloud cover or humidity, temperature changes etc.
- Appropriate number of scans should be taken for each target spectra.
- Noise in the spectra may be routinely checked. Noise may be due to fault in the electronics or the breaks in the cable.
- Instrument should be properly warmed up before starting measurements.
- Now-a-days Spectroradiometers are provided with wireless communication. To avoid communication loss, care must be taken to avoid any RF signal or jammer in the vicinity.

- If field data collection is aimed for validation of hyperspectral image, the timing of data collection should match with that of hyperspectral image so that same illumination conditions must be observed.
- The selection of a particular sampling strategy should be based upon the objectives of the study. If the objective is to develop a spectral library, the required targets should be placed in all expected conditions including background, illumination, slope and aspect, and target surface architecture.
- For hyperspectral image validation, viewing geometry similar to the sensor is required. For developing spectral library, usually, nadir view in direct sunlight is required. Care should be taken to avoid diffuse sunlight.
- The height of data acquisition should be carefully considered and should be in concurrence with the FOV of the instrument.

References

- Anon. (1993). Design and development of Airborne Imaging Spectrometer. SAC/EOSDG/AIS/09/93, Space Applications Centre, Ahmedabad, India.
- Christophe, E., Leger, D., Mailhes, C. (2005). Quality criteria benchmark for hyperspectral imagery. *IEEE transactions on geoscience and remote sensing*. 43 (9), pp 2103-2114.
- Croft, H. and Chen, J.M. (2017). Leaf Pigment Content. Elsevier Inc., Canada. DOI: 10.1016/B978-0-12-409548-9.10547-0
- Dadon, A., Ben Dor, E., Karineli, A. (2009). Correction of spectral curvature effects (smile) in Hyperion datasets by use of derivative calculations and MNF transform. <https://pdf.semanticscholar.org/e382/f4eef03fe6050e3d227541f7517e4720e341.pdf>
- Gao, B., Montes, M.J., Davis, C.O. (2004). Refinement of wavelength calibrations of hyperspectral imaging data using a spectrum-matching technique. *Remote Sensing of Environment V-90*, pp 424-433.
<https://discover.asdi.com/ground-truthing-and-calibration-of-uas>.
https://eo1.gsfc.nasa.gov/new/validationReport/Technology/TRW_EO1%20Papers_Presentations/10.pdf
<http://arsf-dan.nerc.ac.uk/trac/wiki/Reports>
- Janschek, K. and Tchernykh, V. (2001). Optical Correlator for Image Motion Compensation in the Focal Plane of a Satellite Camera. 5th IFAC Symposium on Automatic Control in Aerospace, Bologna.
- Jeffrey, H.W., Chunhua, Z., Jon, M.K. (2014). Separating crop species in North-Eastern Ontario using hyperspectral data. *Remote Sensing*. 6, pp 925-945.
- Jiang, Y., Zhang, G., Tang, X. (2013). Research on the high accuracy band-to-band registration method of ZY-3 multispectral image. *Acta Geodaetica Cartographia Sinica*. 42 (6), pp 884-890.

- Jin, Z. and Stamnes, K. (1994). Radiative transfer in nonuniformly refracting layered media: atmosphere-ocean system. *Applied Optics*. 33(3).
- Jin, Z., Charlock, T.P., Rutledge, K., Stamnes, K. and Wang, Y. (2006). Analytical solution of radiative transfer in the coupled atmosphere–ocean system with a rough surface. *Applied Optics*. 45 (28).
- Kiang, N.Y., Siefert, J., Govindjee and Blankenship, R.E. (2007). Spectral signatures of photosynthesis. I. Review of earth organisms. *Astrobiology*. 7, pp 222–251.
- Kumar Kiran, A.S. (2008). *Hyperspectral Imaging Systems In: Hyperspectral Data, Analysis Techniques and Applications*, Editors-Navalgund, R.R., Ray, S.S. Indian Society of Remote Sensing, Dehradun.
- Moharana, S. and Dutta, S. (2014). Hyperspectral remote sensing of paddy crop using in situ measurements and clustering techniques. *International archival of photogrammetry, remote sensing and spatial information sciences*, doi:10.51.94/isprsarchives-XL-8-845-2014.
- Neville, R.A., Sun, L., Staenz, K. (2008). Spectral calibration of imaging spectrometer by atmospheric absorption feature matching. *Canadian journal of remote sensing*. 34, pp 29-42
- Panigrahy, S., Ray, S.S., Manjunath, K.R., Singh, Rimjhim Bhatnagar, Singh, C.P. and Kumar, T. (2011). *Data Quality Evaluation of Airborne Imaging Spectrometer (AIMS)*, EOAM/SAC/ABHG/HA/SN/01/2011.
- Rose, A. (1973). *Vision Human and Electronic*. Plenum Press. ISBN 9780306307324.
- Sanghvi, C., Ray, S.S. and Singh, Rimjhim Bhatnagar. (2010). A software tool for reflectance spectra analysis In: *Hyperspectral Data, Analysis Techniques and Applications*, Editors-Navalgund, R.R., Ray, S.S. Indian Society of Remote Sensing, Dehradun.
- Singh, Rimjhim Bhatnagar, Ray, S.S. and Panigrahy, S. (2012). *Evaluation of Airborne Imaging Spectrometer (AIMS) data for land applications*, Scientific Report, EOAM/SAC/ABHG/HA/SR/01/2012.
- SPSS Inc. Released 2007. *SPSS for Windows, Version 16.0*. Chicago, SPSS Inc.

Upadhyay, V.P., Misra, P.K. (2008). Population status of mangrove species in estuarine regions of Orissa coast, India. *Tropical Ecology* 49: 183–188.

Wang, M., Yang, B., Jia, S. (2013). A registration method based on object space positioning consistency for satellite multispectral image. *Geomatics and Information science of Wuhan university*. 38 (7), pp 765-769.

www.hico.coas.orgonstate.edu

www.senteksystems.com/2015/11/20/leaf-reflectance-vegetation-indices

Yokoya, N., Miyamura, N. and Iwasaki, A. (2012). Preprocessing of hyperspectral imagery with consideration of smile and keystone properties. In *Multispectral, Hyperspectral, and Ultraspectral Remote Sensing Technology, Techniques, and Applications III*, edited by Allen M. Larar, Hyo-Sang Chung, Makoto Suzuki, *Proc. of SPIE Vol. 7857, 78570B*, doi: 10.1117/12.870437

Zhang, H., Lan, Y., Suh, C.P., Westbrook, J.K., Lacey, R., Hoffman, W.C. (2012). Differentiation of cotton from other crops at different growth stages using spectral properties and discriminant analysis. *Transactions ASABE*. 55, pp 1623-1630.